Heliyon 10 (2024) e27865

Contents lists available at ScienceDirect

Heliyon

journal homepage: www.cell.com/heliyon

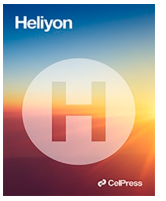

Research article

Single-cell and bulk RNA sequencing highlights the role of M1-like infiltrating macrophages in antibody-mediated rejection after kidney transplantation

Qidan Pang [a,1], Liang Chen [b,1], Changyong An [b], Juan Zhou [a,**], Hanyu Xiao [b,*]

[a] Department of Nephrology, Bishan Hospital of Chongqing Medical University, Chongqing, 402760, China
[b] Department of General Surgery/Gastrointestinal Surgery, Bishan Hospital of Chongqing Medical University, Chongqing, 402760, China

ARTICLE INFO

Keywords:
Macrophage
Antibody-mediated rejection
Single-cell
Kidney transplantation
Graft loss
Biopsies for cause
STAT1
MIF
PARP9

ABSTRACT

Background: Antibody-mediated rejection (ABMR) significantly affects transplanted kidney survival, yet the macrophage phenotype, ontogeny, and mechanisms in ABMR remain unclear.
Method: We analyzed post-transplant sequencing and clinical data from GEO and ArrayExpress. Using dimensionality reduction and clustering on scRNA-seq data, we identified macrophage subpopulations and compared their infiltration in ABMR and non-rejection cases. Cibersort quantified these subpopulations in bulk samples. Cellchat, SCENIC, monocle2, and monocle3 helped explore intercellular interactions, predict transcription factors, and simulate differentiation of cell subsets. The Scissor method linked macrophage subgroups with transplant prognosis. Furthermore, hdWGCNA, nichnet, and lasso regression identified key genes associated with core transcription factors in selected macrophages, validated by external datasets.
Results: Six macrophage subgroups were identified in five post-transplant kidney biopsies. M1-like infiltrating macrophages, prevalent in ABMR, correlated with pathological injury severity. MIF acted as a primary intercellular signal in these macrophages. STAT1 regulated monocyte-to-M1-like phenotype transformation, impacting transplant prognosis via the IFNγ pathway. The prognostic models built on the upstream and downstream genes of STAT1 effectively predicted transplant survival. The TLR4-STAT1-PARP9 axis may regulate the pro-inflammatory phenotype of M1-like infiltrating macrophages, identifying PARP9 as a potential target for mitigating ABMR inflammation.
Conclusion: Our study delineates the macrophage landscape in ABMR post-kidney transplantation, underscoring the detrimental impact of M1-like infiltrating macrophages on ABMR pathology and prognosis.

1. Introduction

Kidney transplantation is the optimal method for renal replacement therapy, yet post-transplant rejection continues to pose significant challenges [1]. In recent decades, advancements in immunosuppressive medications have markedly enhanced early graft

* Corresponding author.
** Corresponding author.
E-mail addresses: zj604050129@163.com (J. Zhou), 142025@cqmu.edu.cn (H. Xiao).
[1] Qidan Pang and Liang Chen contributed equally to this research and share first authorship.

https://doi.org/10.1016/j.heliyon.2024.e27865
Received 28 February 2024; Accepted 7 March 2024
Available online 15 March 2024

survival rates, culminating in over 90% one-year survival rates for transplanted kidneys [2]. However, there has been no substantial improvement in the long-term outcomes of these grafts, with antibody-mediated rejection (ABMR), primarily due to HLA incompatibility between donors and recipients, being the primary cause. Reports indicate that over 60% of long-term kidney transplant failures can be attributed to ABMR [3]. The main culprits behind ABMR are either pre-existing antibodies or newly formed donor-specific antibodies (DSAs). These antibodies result from the activation of B cells or plasma cells by helper T cells, leading to pathological changes characterized by both acute and chronic damage to graft microcirculation and microvascular C4d deposition [4]. Consequently, it is reasonable to assert that adaptive immunity plays a pivotal role in ABMR progression. As a result, current frontline immunosuppressive medications predominantly target the adaptive immune response, where T lymphocytes and B lymphocytes are key actors. However, their efficacy in enhancing long-term graft survival remains limited. Therefore, increasing focus is being placed on the role of innate immune cells in the context of ABMR [5].

As an important component of the innate immune system, macrophages are closely involved in alloimmunity. Prior research found that early infiltration of macrophages in biopsy samples of transplant kidney suggests a worse prognosis [6]. Several clinical studies have shown that in patients with active ABMR, macrophage infiltration in transplanted kidneys is associated with the severity of rejection, deterioration in renal function, and eventual graft failure [7–9]. It had always been believed that macrophages contribute to graft rejection by initiating adaptive immune responses through antigen presentation, providing costimulatory signals, and releasing cytokines.

Exploring the role and mechanisms of macrophages in alloimmunity is a complex endeavor. On one hand, macrophages are highly plastic and heterogeneous, capable of displaying a variety of phenotypic and functional states influenced by the damaged graft microenvironment or temporal effects [10]. On the other hand, the ontogeny of macrophages in allografts is multifaceted. This multi-source is evident not only in the distinction between infiltrating monocyte-derived macrophages and tissue-resident macrophages but also between donor-derived and recipient-derived macrophages. These varying origins significantly influence the functional characteristics of macrophages [11].

Bulk RNA sequencing technology is capable of quantifying gene expression across an entire biological sample, but identifying specific cell types requires the use of deconvolution algorithms. In contrast, single-cell sequencing technology enhances the resolution of the transcriptional landscape to the individual cell level. This approach offers novel insights into the cellular heterogeneity between diseased and healthy tissues, facilitates the discovery of disease-associated biomarkers, and aids in the development of cell-specific targeted therapies [12,13]. In this study, we pinpointed the differential infiltration macrophage populations by comparing single-cell profiles from ABMR and non-rejection biopsy samples, and further investigated the occurrence, cellular interactions, and potential functional mechanisms of these diverse macrophage types through bioinformatics analyses integrated with microarray data.

2. Materials and methods

1 Data Acquisition and Processing

Data Acquisition: We sourced single-cell RNA sequencing and Bulk RNA sequencing data of transplant kidney biopsy tissues, along with corresponding clinical information, from the GEO (Gene Expression Omnibus) and ArrayExpress databases. The datasets included, sample sizes, pathological diagnoses, and links are documented in Supplementary Table 1, [14–19]. These samples were exclusively obtained from indicated biopsies post-kidney transplantation. The pathological diagnoses were based on the Banff criteria. Additionally, we excluded samples with T-cell-mediated rejection and mixed rejection.

Single-cell RNA Sequencing Data Processing: We retrieved barcodes, features, and matrices files from single-cell datasets, processing raw fastq files with Cellranger 7.0. A Seurat object was established using the R Seurat package for data quality control, which involved discarding cells with fewer than 200 gene expressions and those with mitochondrial gene proportions over 20%. We then conducted data standardization and normalization using NormalizeData and ScaleData functions. For dimensionality reduction, PCA was applied to the data using 2000 highly variable genes (HVGs) identified via FindvariableFeatures. To integrate cells from various samples, we utilized the harmony package, followed by cell clustering using Findneighbors and RunUMAP. Differential expression genes between cell clusters were identified with FindAllMarkers, serving as cell cluster-specific markers. These markers were then cross-referenced with the CellMarker [20] database and cell markers from existing literature [21] for accurate cell cluster annotation.

Bulk RNA Sequencing Data Processing: Initially, count data from the series matrix of target samples were retrieved, followed by log2 transformation of the raw, unstandardized data. We then employed the normalizeBetweenArrays function from the R limma package to effectively eliminate batch effects across samples. In the subsequent phase, probe information corresponding to the GPL platform was downloaded. This enabled the conversion of gene probe IDs into a gene symbol format, ensuring consistency and clarity in gene identification. Additionally, comprehensive data encompassing pathological diagnoses, graft survival times, and Banff scores associated with the samples were meticulously collected and documented.

2 Characterization of Macrophage Subgroups

Building on our established single-cell sequencing data processing approach, we further subclassified and annotated the monocyte-macrophage clusters. To elucidate the tissue distribution characteristics of the monocyte-macrophage sub-clusters, we calculated Odds Ratios (ORs) [22] to delineate their distribution preferences. This was followed by a differential analysis of the proportions of various macrophage subgroups within ABMR and non-rejection samples, identifying statistically significant subgroups as Differential Infiltration Macrophages (DIMacs). Moreover, utilizing the methodology proposed by Kaiyu et al. [23], we computed a 'contribution score'

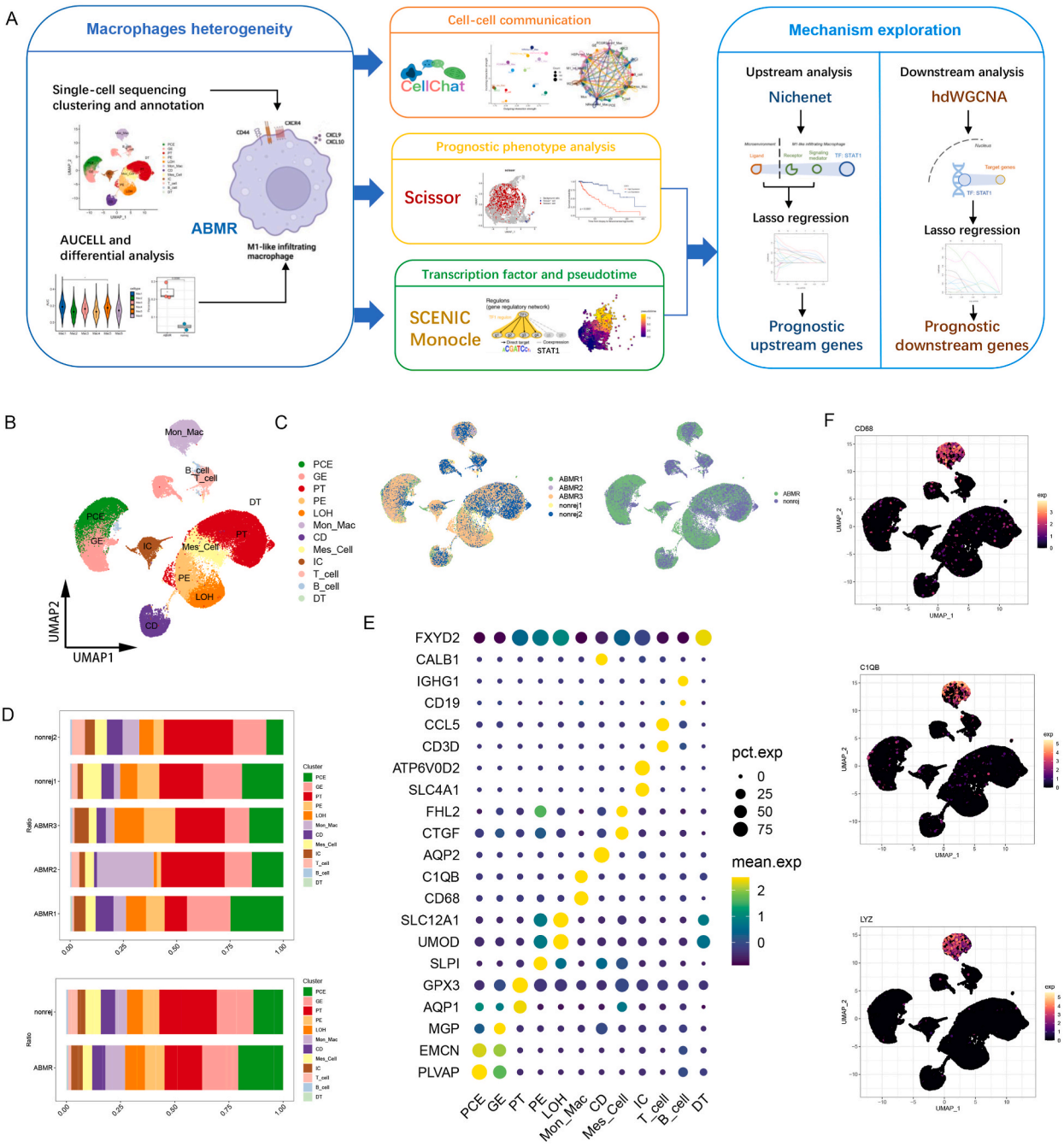

Fig. 1. Landscape of Transplant Microenvironment of Biopsy Samples post Kidney Transplant. (A) Schematic Overview. (B) UMAP illustrating 12 distinct cell clusters derived from three antibody-mediated rejection (ABMR) and two non-rejection cases. PCE, peritubular capillary endothelium cells; GE, glomerular endothelium cells; PT, proximal tubular cells; PE, pelvic epithelial cells; LOH, loop of Henle cells; CD, collecting ductal cells; Mes-cell, mesangial cells; IC, intercalated cells; DT, distal tubular cells; Mon-Mac: monocyte-macrophages. (C) UMAP showcasing the distribution of these cell clusters within the biopsy samples. (D) Proportion of each cell cluster in biopsy samples. (E) Dot plot representation of characteristic marker genes for each cell cluster. (F) Detailed visualization of distribution and expression patterns for three key monocyte-macrophage markers: CD68, C1QB, and LYZ.

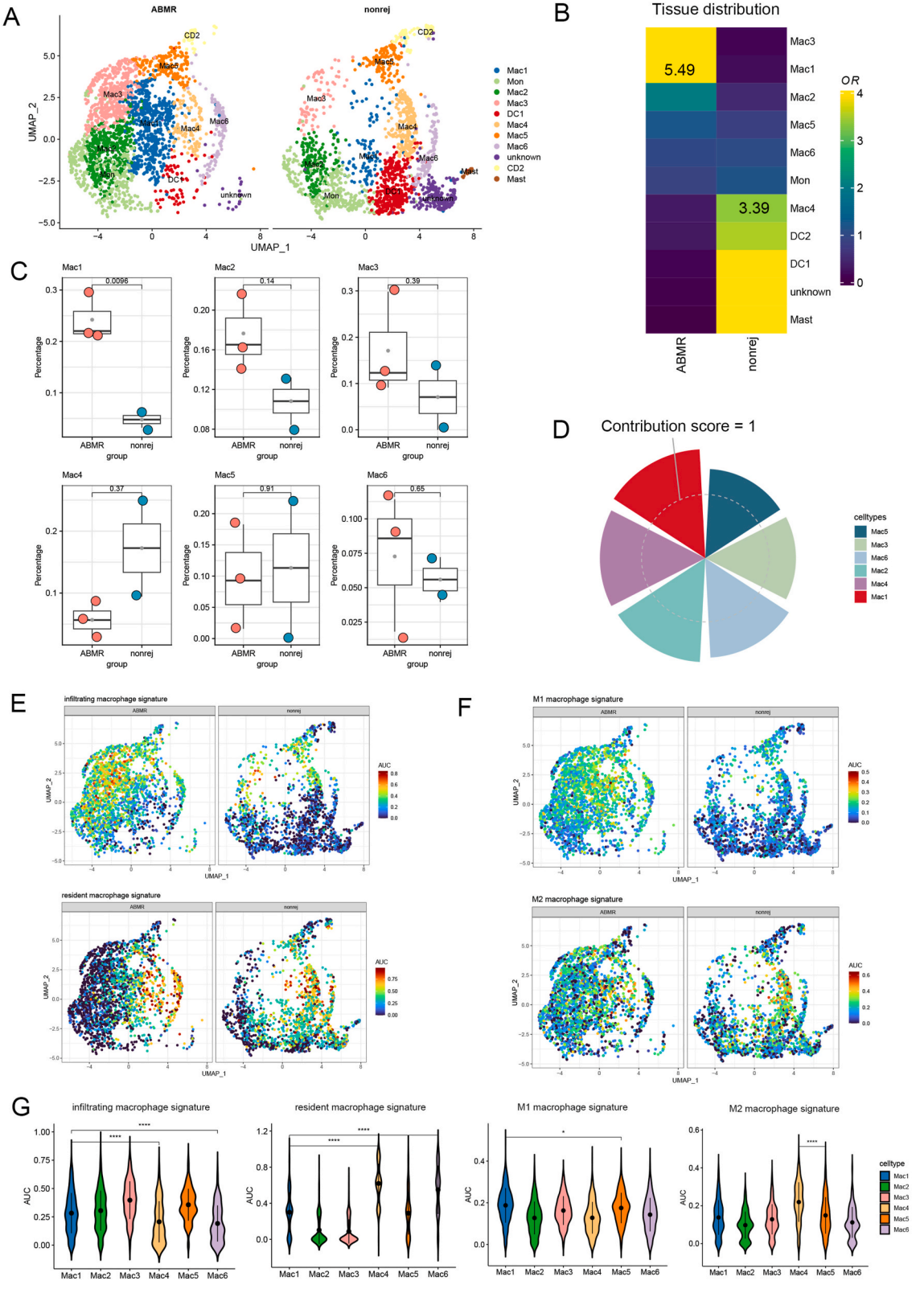

(caption on next page)

Fig. 2. Detailed Analysis of Macrophage Subclusters in ABMR and Non-Rejection Kidney Transplant Samples. (A) UMAP delineating monocyte-macrophage (Mon-Mac) subclusters, comparing antibody-mediated rejection (ABMR) and non-rejection cases. (B) Heatmap illustrating the distribution preferences of Mon-Mac subclusters across samples (indicated by OR values). (C) Comparative analysis of the infiltration percentages of macrophage subclusters in ABMR versus non-rejection samples. (D) Radial graph displaying the contribution scores of each macrophage subcluster to ABMR, with a dashed line indicating the baseline score of 1 for reference. (E) and (F) UMAPs highlighting the area under curve (AUC) values and distribution patterns of macrophage-related phenotypic signatures in ABMR versus non-rejection samples. (G) Violin plots providing a comparative overview of each signature's AUC score across different macrophage subclusters.

to quantify each macrophage subgroup's impact on the disease process. In identifying the phenotypic profiles of these macrophage subgroups, we extracted infiltrating and resident macrophage signatures, alongside M1 and M2 macrophage signatures, from the existing literature [24,25]. The activity level of phenotypic signatures in each cell was calculated using the AUcell package, as detailed in Supplementary Table 2. The sub-clusters were annotated based on these AUcell results, complemented by cell cluster-specific markers. Additionally, this refined data processing protocol was consistently applied to the single-cell validation dataset.

Finally, the R pheatmap package was employed to display the top 20 cell markers for each sub-cluster. We conducted a Gene Ontology (GO) analysis through ToppGene Suite [26], with the results showcased in a dot plot format. Our focus was particularly directed towards macrophage-related genes, encompassing MHC, pro-inflammatory, and anti-inflammatory genes. To this end, we computed their average expression levels within the sub-clusters. In addition, we utilized the R GSVA package to ascertain the enrichment scores of each sub-cluster within the inflammation-related Hallmark pathways. The outcomes of these analyses were effectively visualized using heatmaps.

Moreover, we used the Cibersort [27] deconvolution algorithmto determine the infiltration of specific types of macrophages within the Bulk RNA seq dataset, thereby validating the differences in their proportions between ABMR samples and non-rejection samples. According to the Banff criteria, the pathological injury scores used for diagnosing ABMR primarily include the following five metrics [28]: Glomerulitis (g0~g3), Peritubular Capillaritis (ptc0~ptc3), Arterial Inflammation (v0~V3), C4d (c4d0~ c4d 3), and Transplant Glomerulopathy (cg0~cg3). We collected the pathological injury scores of samples from the GSE98320 dataset and employed t-tests and Kruskal-Wallis tests to compare the proportions of DIMacs infiltration under different injury scores. This analysis aimed to explore the relationship between macrophage infiltration and the extent of pathological injury.

3 Characteristic Analysis of Differentially Infiltrated Macrophages

To delve into the intricacies of cellular crosstalk, we utilized the CellChat [29] package for deducing and analyzing intercellular communication networks from scRNA-seq data. In this endeavor, the cellphoneDB [30] database served as reference dataset. Our focus was on identifying critical ligand-receptor pairs and signaling pathways that facilitate communication between DIMacs and the key effector cells in antibody-mediated rejection, namely T cells and B cells, as well as the principal cells involved in injury, the endothelial cells.

The SCENIC [31] packageis utilized for the inference of Gene Regulatory Networks (GRNs) within specific macrophage subgroups and for pinpointing the transcription factors (TFs) that govern these networks. In line with the SCENIC pipeline, the GENIE3 method and RcisTarget are applied to identify potential TFs, and the regulon activity was generated by AUCell.

We advanced our investigation by tracing the differentiation trajectories of macrophage subgroups, with a particular focus on DIMacs. To begin, the monocle3 [32] package was used to chart the direction of cell differentiation, guided by identified biological developmental starting points. Following this, we employed monocle2 [33] (method = "DDRTree", ordering genes = marker genes) to map out the pseudotime trajectories for individual cells. Finally, we depicted the variations in gene expression of phenotypic genes and core TFs within DIMacs across the pseudotime.

The Scissor [34] package used to identify cell subgroups related to transplant prognosis phenotypes and to simulate the correlation between phenotypes and cells through regression models. Cells positively correlated with the graft loss phenotype are classified as high-risk cells (HR cells), while those negatively correlated are deemed low-risk cells (LR cells). Cells with no significant correlation are categorized as background cells. Additionally, we compared the proportions of HR cells to non-HR cells within DIMacs to investigate the differences in gene expression between high and low-risk cells. Further, differential genes were subjected to enrichment analysis using Metascape.

4 Upstream and Downstream Analysis of Core Transcription Factors in DIMacs

Following the analytical workflow of the hdWGCNA [35] package, we constructed gene co-expression networks using scRNA-seq data from infiltrating macrophage subgroups. We selected co-expression modules that exhibited the highest overlap with DIMacs gene expression. The top 100 module eigengenes (MEs) with the highest eigengene-based connectivity (kMEs) were identified as candidate downstream genes. Further analysis in Cytoscape was performed using the iRegulon [36] plugin to predict core TF regulating these downstream genes. We then divided randomly the prognosis dataset GSE21374 into a training set and a test set in a 1:1 ratio. Cox regression was used to identify prognostic downstream genes (PDGs). Subsequent lasso regression helped to pinpoint critical PDGs and construct a prognostic risk prediction model. The model utilized gene expression levels as parameters and regression coefficients as gene coefficients, calculating risk scores with the formula: $RiskScore = \sum_{i=1}^{n}(coef_i * expr_i)$. The survminer package was employed to plot Kaplan-Meier survival curves, using the Log Rank test to compare transplant survival differences between high and low-risk

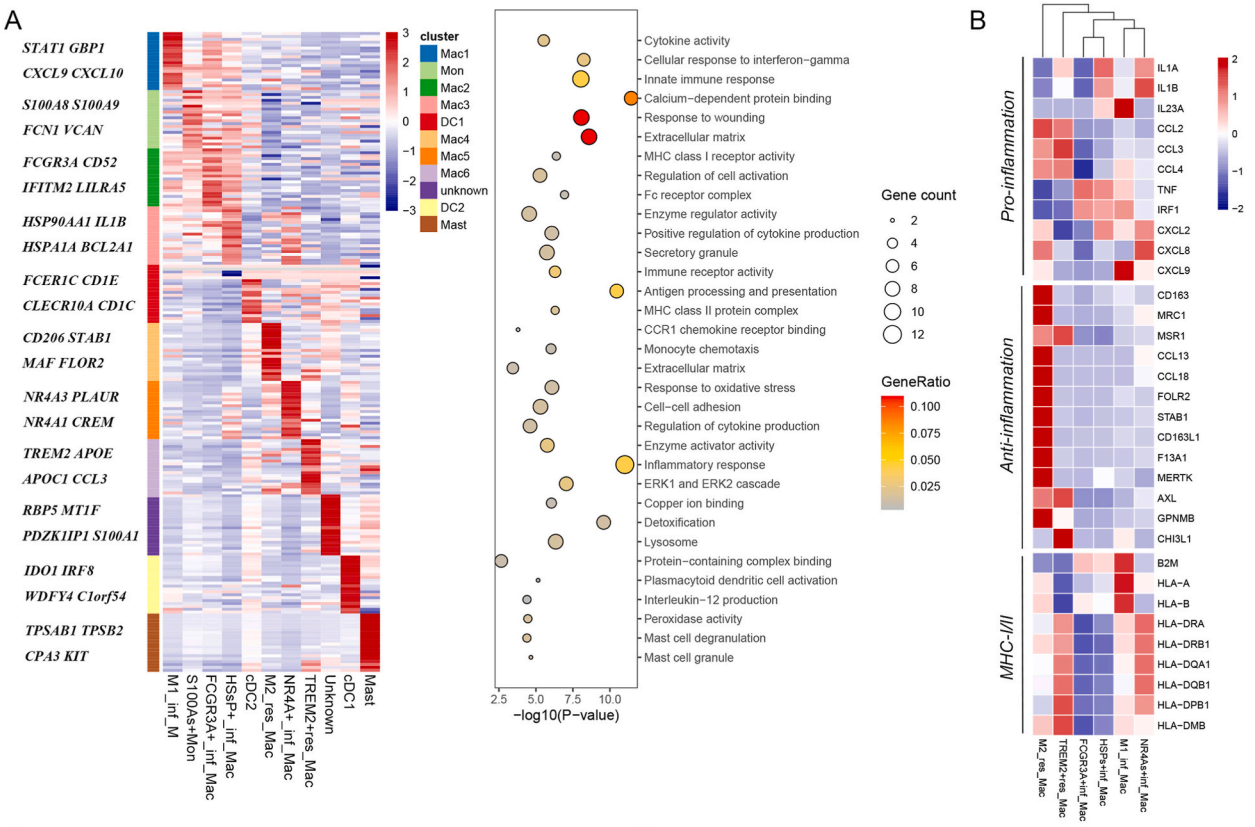

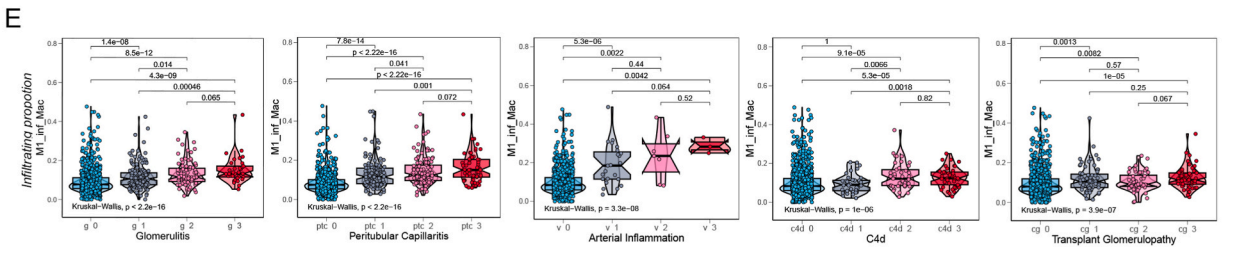

(caption on next page)

Fig. 3. Transcriptomic Profiling of Macrophage Subclusters and Integration with Bulk RNA Sequencing Data. (A) Left: Heatmap displaying the top 20 cell-special genes in each cell cluster, with gene expression values represented as row-scaled Z-scores. Right: Key Gene Ontology (GO) terms associated with these genes. (B) Heatmap of the expression patterns of macrophage-related genes across different macrophage subclusters. (C) Heatmap illustrating Gene Set Variation Analysis (GSVA) scores for inflammatory hallmark signaling pathways in macrophage subclusters. (D) Estimated proportion of M1-like infiltrating macrophage in ABMR versus non-rejection, based on datasets GSE36059 and GSE98320. (E) Infiltrating proportion of M1-like infiltrating macrophages in ABMR-related pathological lesion.

groups. The timeROC package was used to draw ROC curves to evaluate the predictive performance of the model.

NicheNet [37] is a computational method that simulates how intercellular interactions influence gene expression in cells. It integrates single-cell gene expression data with a priori knowledge of gene regulatory networks to model authentic cell-to-cell communication processes: ligand – receptor - signaling protein - transcription regulator - target gene. Using the nichenetr package, we constructed interaction networks between DIMacs and endothelial cells, as well as immune cells (with DIMacs as the receiver, and endothelial and immune cells as the senders). We identified potential ligands of core TF (regulatory potential score >0.01) and their upstream receptors or signaling proteins. Similar to the analysis process for downstream analysis, we employed Cox regression and Lasso regression to identify key upstream genes affecting prognosis, and then developed and validated a corresponding model.

5 Correlation Analysis Between Core Transcription Factors and Associated Genes

To explore the relationships between core TF and their upstream and downstream genes, as well as their correlations with DIMacs infiltration, we performed Pearson correlation analysis using the R 'cor' function on the transcriptome datasets GSE36059 and GSE98320. For the downstream genes of particular interest, their distribution in relation to upstream genes and core transcription factors was depicted on a UMAP two-dimensional plane using single-cell data, with a specific focus on assessing their correlations within DIMacs. Ultimately, we conducted a validation of crucial upstream-TF-downstream pathways in a separate ABMR single-cell dataset.

3. Results

1 Single-Cell Profiling of the Transplant Microenvironment Landscape in ABMR versus Non-Rejection

In this study, five for-cause biopsy samples post-kidney transplantation were examined, among which three were pathologically diagnosed as Antibody-Mediated Rejection (ABMR) cases, including two active ABMR and one chronic active ABMR, and the remaining two as non-rejection cases. The experimental procedure is schematically illustrated in Fig. 1A. After stringent single-cell data quality control and filtering, a total of 60,971 cells were obtained from these samples. Through unsupervised clustering, these cells were mapped onto a UMAP two-dimensional axis plane into 12 distinct cell populations. This included renal tissue cells such as peritubular capillary endothelium cells (PCE), glomerular endothelium cells (GE), proximal tubular cells (PT), pelvic epithelial cells (PE), loop of Henle cells (LOH), collecting ductal cells (CD), mesangial cells (Mes-cell), intercalated cells (IC), and distal tubular cells (DT), as well as immune cells such as monocyte-macrophages (Mon-Mac), T cells, and B cells, as depicted in Fig. 1B. The distribution of these cell clusters was relatively uniform across the samples, showing no evident sample-specific characteristics (Fig. 1C). The marker genes for each cell type and their expression patterns are presented in a bubble plot (Fig. 1E). Monocyte-macrophages were observed to constitute the highest proportion within the immune cell clusters and exhibited more abundant infiltration in the ABMR samples compared to the non-rejection samples (Fig. 1D). The UMAP plot in Fig. 1F displays the distribution and expression of three marker genes of the monocyte-macrophage cluster (CD68, C1QB, LYZ).

2 Characteristic and Heterogeneity of Macrophages in ABMR versus Non-Rejection

Upon further sub-grouping of monocyte-macrophages, we identified 11 cell subpopulations (Fig. 2A), including one monocyte subpopulation (Mon), six macrophage subpopulations (Mac1-Mac6), two dendritic cell subpopulations (DC1-DC2), one mast cell subpopulation (Mast), and one unidentified subpopulation (unknown). analysis revealed that Mac1 predominantly localized in ABMR samples ($OR = 5.49$, $P < 0.01$), while Mac4 showed a preference for non-rejection samples ($OR = 3.39$, $P < 0.01$) (Fig. 2B). In the differential analysis, Mac1 was significantly more prevalent in ABMR than in non-rejection samples ($P < 0.001$), indicating that Mac1 represents differential infiltration macrophages (DIMacs); however, the differences in other subpopulations like Mac4 were not significant between the two groups (Fig. 2C). Furthermore, Fig. 2D indicates that Mac1 contributes most significantly to the pathogenesis of ABMR, followed by Mac4.

We analyzed the phenotypic differences among the macrophage subgroups and found that Mac1, Mac2, Mac3, and Mac5 exhibited distinct infiltrating cell phenotypes, while Mac2 and Mac4 demonstrated tissue-resident cell phenotypes (Fig. 2E and G). Mac1 showed a particularly prominent M1 macrophage phenotype, and Mac4 showed a notable M2 macrophage phenotype (Fig. 2F and G). Based on these characteristics, we designated Mac1 as M1-like infiltrating macrophages (M1-inf-mac) and Mac4 as M2-like resident macrophages (M2-res-mac). The pronounced phenotypic features and their substantial contributions to the disease led us to hypothesize that these two subgroups are the primary effector macrophages in ABMR.

The heatmap in Fig. 3A displays annotations for the specific cell types of the 11 cell subpopulations, integrating the top 20 cell-

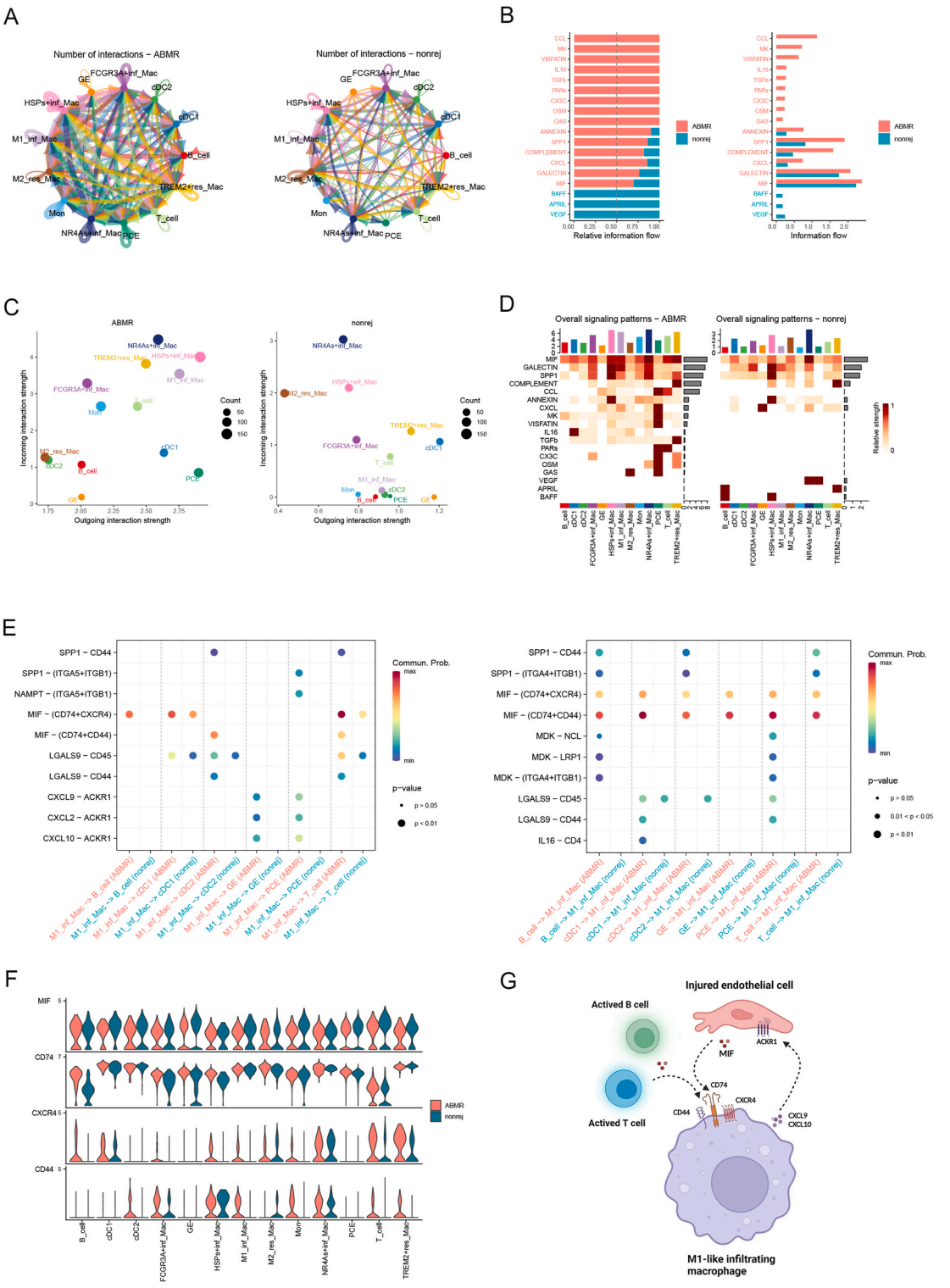

Fig. 4. Cell-cell Communication among Macrophage Subclusters. (A) Visualization of cell interaction networks, contrasting ABMR with non-rejection samples. Line thickness indicates the number of interactions between cells. (B) Differences in the overall signaling pathway between ABMR and non-rejection samples. (C) Depiction of incoming and outgoing interaction strengths between cells in ABMR versus non-rejection samples. Circle sizes represent the intensity of these interactions. (D) Heatmap illustrating the overall signaling patterns in ABMR and non-rejection samples, with color shades indicating the relative strength of different signaling pathways. (E) Communication probabilities of important ligand-receptor pairs between M1-like infiltrating macrophages and effective cells in ABMR. Dot colors show communication probability, while

dot sizes indicate p-values. (F) Violin plot comparing the expression of genes in the MIF signaling pathway across subclusters in ABMR and non-rejection samples. (G) Exploration of potential crosstalk between M1-like infiltrating macrophages and other cell types, including T cells, B cells, and endothelial cells, in the transplant microenvironment.

special markers and phenotypic analysis results, along with the Gene Ontology (GO) analysis outcomes for these subpopulations' characteristic genes. We discovered that the characteristic genes of M1-inf-mac are mainly enriched in terms related to cytokine activity, cellular response to interferon-gamma, and innate immune response. They also show high expression of MHC-related genes (B2M, HLA-A, and HLA-B), and pro-inflammatory genes (TNF, IRF1, and IL23A) (Fig. 3B). The characteristic genes of M2-res-mac correspond to CCR1 chemokine receptor binding, monocyte chemotaxis, extracellular matrix, and show high expression of anti-inflammatory genes (CD163, MRC1, CCL13, CCL18, FOLR2, STAB1). In the hallmark pathway analysis, genes of M1-inf-mac are primarily enriched in the IFN-α/γ and IL6-JAK-STAT3 pathways (Fig. 3C), while those of M2-res-mac are mainly associated with angiogenesis and epithelial-mesenchymal transition pathways. These enrichment analysis results are consistent with the aforementioned phenotypic analyses.

In the external bulk-RNA seq datasets GSE36059 and GSE98320, we validated the significantly higher infiltration of M1-inf-mac in ABMR samples using a deconvolution algorithm (Fig. 3D). Conversely, M2-res-mac showed no strong infiltration or reduced infiltration in ABMR (Supplementary Fig. 1A). Additionally, in our pathological analysis related to ABMR, we observed that in the five main pathological lesions, the infiltration proportion of M1-inf-mac significantly increased with the escalating Banff scores (Fig. 3E). This suggests a close correlation between the infiltration of M1-inf-mac and the severity of ABMR damage. However, no clear pattern was evident between M2-res-mac and the pathological lesions (Supplementary Fig. 1B). Therefore, M1-inf-mac plays a more significant role in ABMR injury compared to M2-res-mac.

3 MIF is a Crucial Intermediary for M1-inf-mac Interaction with Other Cells in ABMR

Utilizing Cellchat to model the intricacies of cell-to-cell signaling, our analysis revealed a markedly increased frequency of interaction between immune cells and endothelial cells in ABMR compared to non-rejection scenarios (Fig. 4A). The predominant signaling motifs in ABMR involved pathways like CCL, IL16, TGFb, SPP1, COMPLEMENT, CXCL, and notably MIF, whereas VEGF and BAFF signaling were more prominent in non-rejection cases (Fig. 4B). Notably, in ABMR, infiltrating macrophages, specifically M1-inf-mac, HSPs-inf-mac, and NR4A-inf-mac, demonstrated enhanced output and input interaction strengths (Fig. 4C). Fig. 4D illustrates the detailed signaling interactions between immune cells and endothelial cells, highlighting that in ABMR, M1-inf-mac chiefly employs communication pathways such as MIF, GALECTIN, SPP1, and CXCL, with these signals being significantly stronger than in non-rejection. We mapped the interactive pathways of M1-inf-mac with other cells (Fig. 4E): in ABMR, M1-inf-mac predominantly utilizes the MIF-CD74-CXCR4 axis to relay signals to T cells, B cells, and dendritic cells. Concurrently, the MIF-CD74-CXCR4/CXCR4 pathway functions as an inbound signaling mechanism from T cells, B cells, and dendritic cells to M1-inf-mac. Thus, MIF emerges as a pivotal mediator in the interaction of M1-inf-mac with other immune cells within the ABMR context. Regarding endothelial cells, M1-inf-mac induces inflammatory responses by discharging CXCL9 and CXCL10, which interact with ACKR1 on the endothelial surface. Additionally, endothelial cells attract M1-inf-mac infiltration via the MIF pathway (Fig. 4G). The expression profiles of key genes within the MIF signaling pathway are depicted in Fig. 4F. Notably, M1-inf-mac exhibits high expression of the receptor protein gene CD74, and in ABMR, genes for downstream signaling molecules like CD44 and CXCR4 are significantly upregulated compared to non-rejection cases.

4 STAT1 Plays a Vital Regulatory Role in M1-inf-mac and Induces the Transformation of S100As + Mon into this Subtype

SCENIC analysis indicated differential expression of transcription factors across various macrophage subpopulations. Notably, STAT1, IRF1, and IRF7 were enriched in M1-inf-mac, with STAT1 exhibiting the highest regulatory activity in this subgroup (Fig. 5A). Fig. 5B depicts a t-SNE plot of the macrophage subgroups, based on the activity levels of transcription regulatory factors. It was observed that the M1-inf-mac subgroup displayed the most robust regulatory activity of STAT1.

We conducted a pseudotime analysis of the monocyte-macrophage subpopulations (Supplementary Figs. 2A and B). Along the pseudotime trajectory, the cell lineage bifurcates at node 3 into two branches, with M1-inf-mac and M2-res-mac occupying the endpoints of these respective branches. This suggests the existence of two distinct differentiation paths within the macrophage subgroups: the M1-inf-mac fate and the M2-res-mac fate. FCGR3A + inf-mac, HSPs + inf-mac, and NR4As + inf-mac represent intermediate states in the cell differentiation process (Supplementary Fig. 2C). The characteristic genes of M1-inf-mac (CXCL9, CXCL10, and STAT1) and those of M2-res-mac (MRC1, STAB1, and MAF) exhibit divergent expression trends over pseudotime (Supplementary Figs. 2D and 2E).

Considering the biological origins of infiltrating macrophages, we proposed that S100As + Mon serves as the initial stage in the M1-inf-mac fate. This hypothesis was substantiated by pseudotime analysis, which delineated the differentiation trajectory from S100As + Mon through FCGR3A + inf-mac to M1-inf-mac (Fig. 5C). Fig. 5D illustrates the expression dynamics over pseudotime for transcription factors STAT1, IRF1, and IRF7, as well as for CD86, a gene indicative of the M1 macrophage phenotype. A notable parallel in the expression trends of STAT1 and CD86 was observed, both exhibiting a steadily ascending curve with the progression of pseudotime. The heatmap reveals the temporal expression patterns of differential genes, showing heightened expression of the MIF pathway signaling molecule CD74, MHC-II genes (HLA-DR, HLA-DC), inflammatory mediators (GBP1, GBP5, CXCL9, CXCL10), and chemokines

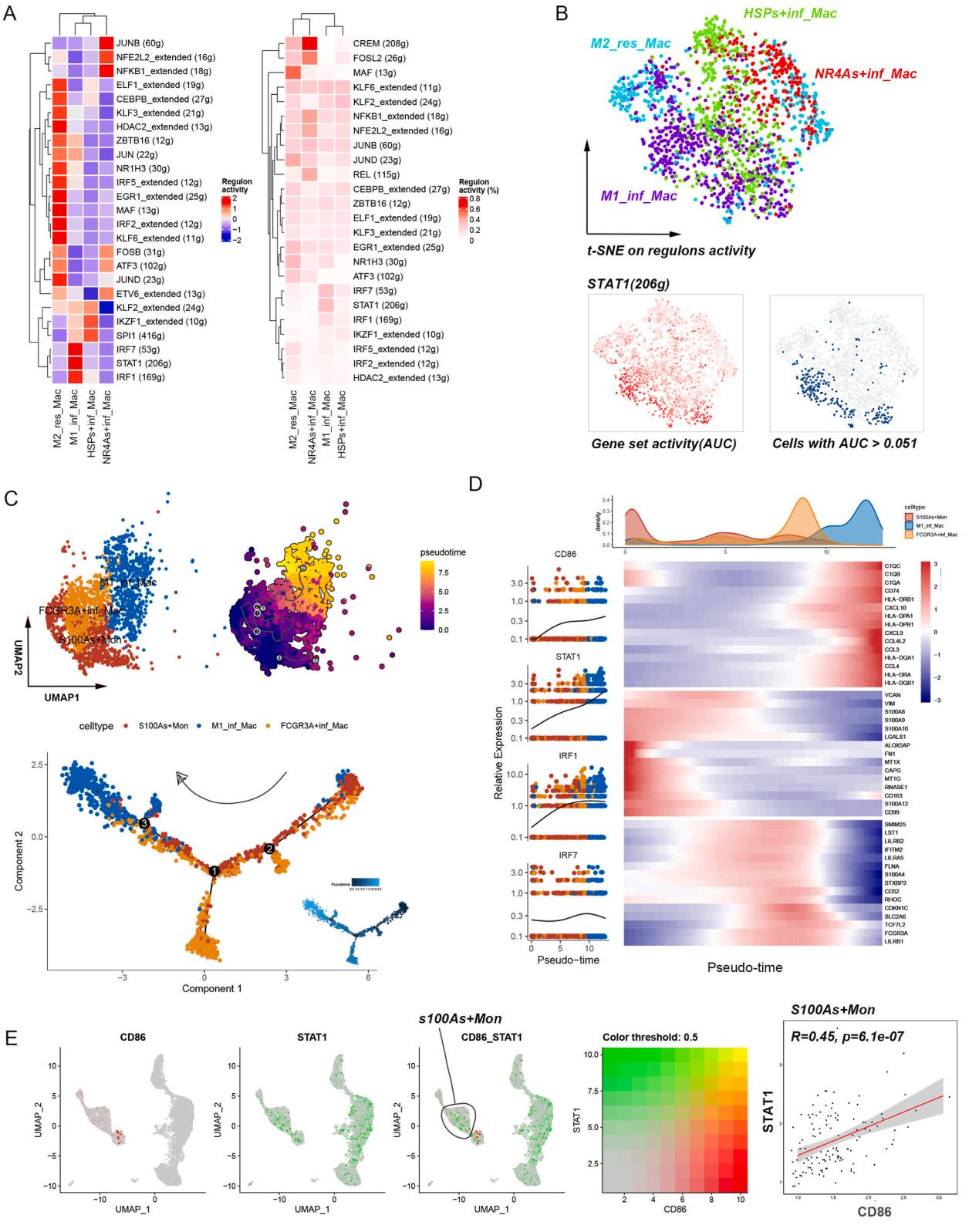

(caption on next page)

Fig. 5. Transcription Factor Prediction and Pseudotime Analysis of Macrophage Subclusters. (A) Heatmap representing the regulon activity (%) in various macrophage subclusters. (B) Analysis of the distribution and activity levels of STAT1 within M1-like infiltrating macrophages. (C) Pseudotime and trajectory of monocyte-derived cell lineage (S100A + monocytes, FCGR3A + infiltrating macrophages, and M1-like infiltrating macrophages). (D) Comprehensive overview of cell lineage dynamics: Top panel shows cell density variations among monocyte-derived subtypes during pseudotime. Bottom left panel presents a pseudo-heatmap of representative differentially expressed genes (DEGs) along the trajectory. Bottom right panel details the expression variation and distribution of selected transcription factors (TFs) and phenotypic genes throughout the pseudotime. (E) UMAP highlighting the coordinated expression of CD68 and STAT1 in S100A + monocytes derived from recipients' peripheral blood.

(CCL3, CCL4) in the later stages of M1-inf-mac development. In the peripheral blood mononuclear cells of recipients with ABMR samples, S100As + Mon was also detected, demonstrating a significant positive correlation between STAT1 and CD86 (Fig. 5E). This finding indicates the potential for recruitment and differentiation of S100As + Mon into M1-inf-mac within the transplanted kidney, suggesting a pivotal role for STAT1 in this conversion process. Interestingly, M2-res-mac occupies the initial and final points of the differentiation trajectory that interconverts with M1-inf-mac, with NR4As + inf-mac and HSPs + inf-mac representing transitional states (Supplementary Fig. 2F). Additionally, TREM2+res mac seems to be a major differentiation precursor for M2-res-mac (Supplementary Fig. 2G).

5 Infiltration of M1-inf-Mac predicts poor graft outcomes after kidney transplant

Considering the distinct infiltration of M1-inf-Mac in ABMR and its association with the degree of pathological damage, we postulated that the presence of M1-inf-Mac could adversely affect the survival of transplant grafts. Analysis using the Scissor indicated that high-risk (scissor+) cells were predominantly located within the M1-inf-Mac subgroup (Supplementary Fig. 3A). Furthermore, a significantly higher proportion of high-risk cells was observed in the M1-inf-Mac subgroup compared to the background cells ($P < 0.01$) (Supplementary Fig. 3B). A gene expression analysis contrasting high-risk cells with non-risk cells within M1-inf-Mac revealed notable upregulation of genes such as CXCL10, GBP1, CXCL9, IFITM1, TNFSF10, and STAT1 in high-risk cells (Supplementary Figs. 3C and 3E), primarily involved in the INF-γ pathway (Supplementary Fig. 3D). Survival analyses showed that grafts with high M1-inf-Mac infiltration exhibited significantly lower survival rates than those with lower infiltration levels ($P < 0.001$) (Figure Supplementary 3F). Additionally, a higher proportion of high-risk cells was also observed in M2-res-mac ($P < 0.05$) (Supplementary Fig. 3B). Grafts with high infiltration of M2-res-mac were correlated with poorer survival rates ($P = 0.017$) (Supplementary Fig. 3G), where the prognostic differential genes were mainly enriched in lipid metabolism and atherosclerosis pathways (Supplementary Fig. 3H).

6 Upstream and Downstream Genes of STAT1 in M1-inf-mac Can Predict Graft Prognosis

The subtypes of infiltrating macrophages, with their pro-inflammatory characteristics, might play a synergistic role in the progression of ABMR. We constructed a gene co-expression network for infiltrating macrophages using hdWGCNA (Fig. 6A), where the green module (Fig. 6C) showed a significant association with M1-inf-Mac (Fig. 6B). Enrichment analysis revealed that core genes in the green module were primarily concentrated in the INF-γ pathway (Fig. 6D) and were highly expressed in HR cells (Fig. 6B). Identifying transcription factors regulating the genes in the green module, we found STAT1 to be the core regulon with the most regulatory genes, aligning with previous findings; the network of STAT1 and its regulated downstream genes is depicted in Figure Supplementary 4A. We employed Cox regression (Supplementary Fig. 5) and lasso regression (Fig. 6F and G and Supplementary Table 2) to identify five critical prognostic downstream genes: GBP1, HLA-E, PARP9, PSMB8, and TNFSF10 (Fig. 6E). Using these critical PDGs, we developed a, where the high-risk group showed significantly worse survival rates than the low-risk group (training set: $P = 0.001$; test set: $P < 0.001$) (Supplementary F. 4B and F. 6H); the prognostic risk model demonstrated robust predictive performance (training set AUC of 3, 5, 10-year survival: 0.73, 0.78, 0.73; test set AUC of 3, 5, 10-year survival: 0.92, 0.89, 0.92) (Supplementary F. 4C and F. 6I). In datasets GSE36059 and GSE98320, the expression of critical PDGs in ABMR was significantly higher than in non-rejection (Supplementary Figs. 4E and 4F). Dot plots show that critical PDGs are highly expressed in M1-inf-Mac and HR cells (Supplementary Figs. 4G and 4H).

By employing Nichnet, we established a ligand-receptor-signaling mediators-STAT1 communication network, as depicted in Fig. 7A. In this network, receptors and signaling mediators are classified as STAT1's upstream genes. Through Cox (Supplementary Fig. 6) and lasso regression (Fig. 7B and C and Supplementary Table 2) analyses, we identified eight critical prognostic upstream genes: ITGB1, TLR2, TLR4, CD74, PLAUR, ADAM17, CSF1R, and CD81 (Fig. 7A). Building upon these critical PUGs, a prognostic risk model was developed, which distinctly demonstrated that the survival rates were significantly lower in the high-risk group compared to those in the low-risk group (training set: $P < 0.001$; test set: $P < 0.001$) (Fig. 7D and Supplementary Fig. 4I). This prognostic risk model exhibited excellent predictive accuracy, with the training set AUC for 3, 5, and 10-year survival being 0.84, 0.82, and 0.86, respectively, and the test set AUC being 0.85 for both 3 and 5-year survival, and 0.77 for 10-year survival. Dot plots revealed a heightened expression of these critical PUGs in HR cells (Fig. 7F and Supplementary Fig. 4J). Furthermore, the dataset GSE98320 validated the significantly higher expression of these critical PUGs in ABMR compared to non-rejection cases (Fig. 7G).

7 PARP9 as a Novel Regulator of M1-inf-mac Through STAT1 in ABMR

In pursuit of deeper insights into the links between the identified upstream and downstream genes and STAT1, we undertook a comprehensive correlation analysis. At the cellular level, significant positive correlations were found between M1-inf-mac and these genes within the datasets GSE36059 and GSE98320 (Fig. 8A). Genetically, a majority of the genes exhibited close interconnections,

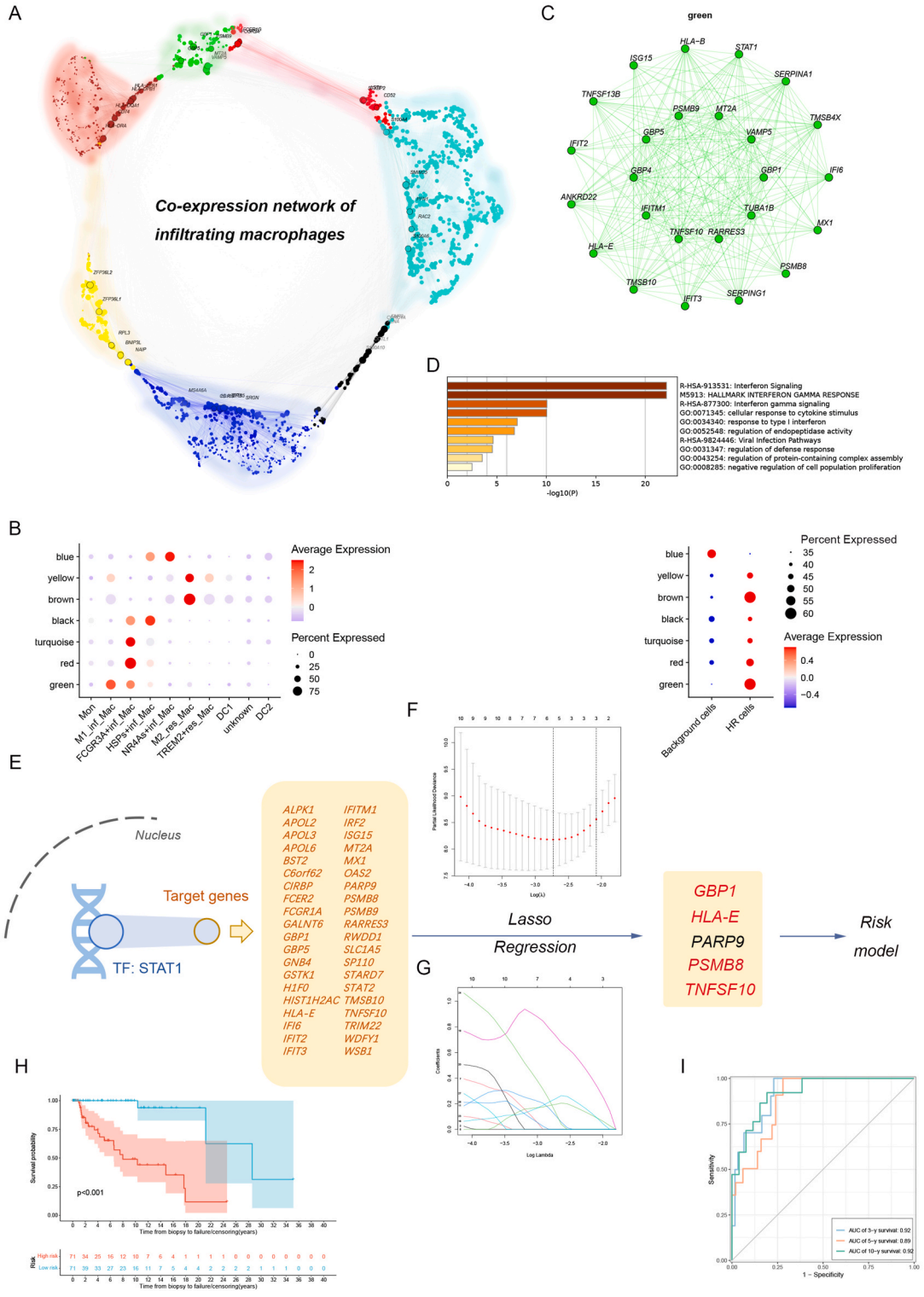

Fig. 6. Development and Validation of a Prognostic Prediction Model Based on STAT1 Downstream Genes. (A) Illustration of the co-expression network of infiltrating macrophages derived from hierarchical weighted gene co-expression network analysis (hdWGCNA). (B) Dot plot showcasing the similarity in gene expression between co-expression modules and various cell clusters or prognostic phenotypes. (C) Top20 hub genes within green module. (D) Enrichment analysis results for the top hub genes in the green module. (E) Schematic overview of the procedure for constructing the prognostic risk model. The left box details the identification of prognostic downstream genes (PDGs) via Cox regression analysis. The right box illustrates the selection of critical PDGs through Lasso regression. Genes highlighted in red are those whose roles in kidney

transplantation have been verified in published literature. (F) Lasso coefficient profiles of the model. (G) Plot depicting the partial likelihood deviance for model optimization. (H) Kaplan-Meier (K–M) survival curve comparing graft survival between high-risk and low-risk groups in the test set. (I) Receiver operating characteristic (ROC) curve analysis of the model, displaying the area under the curve (AUC) for 3-year, 5-year, and 10-year graft survival predictions in the test set.

with TLR4, STAT1, and PARP9 showing a notable positive correlation (Fig. 8B). The TLR4-STAT1-PARP9 signaling axis, not previously reported in the literature, thus became a focus of our further investigations. Our single-cell data revealed that TLR4 and PARP9 are concurrently expressed in M1-inf-mac, displaying a significant positive correlation ($R = 0.44$, $P = 0.012$). Furthermore, the gene expressions of TLR4 and PARP9 were also found to be closely related ($R = 0.3$, $P = 0.00066$) (Fig. 8C). Additionally, within M1-inf-mac, PARP9's expression showed significant positive correlations with pro-inflammatory genes (TNF, CCL2, and CXCL10), the IFNγ receptor gene (IFNR2), and IFNγ stimulated genes (TNFSF10 and IFITM1) (Fig. 8D). This suggests an association of PARP9 with the IFNγ pathway. Existing research confirms that PARP9, by inhibiting the ADP-ribosylation of STAT1, facilitates the activation of inflammatory macrophages and bolsters IFNγ-induced immune responses [38]. STAT1 serves as a nexus between the TLR4 and IFNγ pathways [39]. Consequently, we propose that in M1-inf-mac, upstream signals from TLR4, synergizing with IFNR, initiate the phosphorylation of STAT1, resulting in augmented transcription of PARP9. This action of PARP9, inhibiting STAT1 ADP-ribosylation and promoting its nuclear translocation, intensifies the transcription of ISGs and pro-inflammatory genes, ultimately leading to the inflammatory activation of M1-inf-mac (Fig. 8E).

To corroborate our discoveries and conjectures, we undertook an analysis of single-cell data from two ABMR samples within an independent dataset, employing an identical analytical process. Post-data processing, the cells were categorized into nine distinct types (Fig. 9A), with cluster 7, characterized by high expression of CD68 and LYZ (Fig. 9B), identified as a monocyte-macrophage subgroup. Following another round of unsupervised clustering, we identified four cell subpopulations consistent with our prior analysis — M1-inf-mac, M2-res-mac, FCGR3A + inf-mac, and S100As + mon — and additionally, a novel macrophage subgroup, FOLR2-res-mac, as well as a noise cell subgroup, B cells (Fig. 9C). The marker genes of these subgroups are displayed in Fig. 9D. Notably, Fig. 9E shows the M1 macrophage signature activity prominently in M1-inf-mac, and similarly, M2 macrophage signature activity was significantly observed in M2-res-mac, validating our cell annotations. The expression of STAT1 and associated upstream/downstream prognostic genes was notably elevated in M1-inf-mac and its precursor, FCGR3A + inf-mac (Fig. 9F). Furthermore, TLR4 and PARP9, as well as STAT1 and PARP9, demonstrated synergistic expression and significant positive correlation within M1-inf-mac.

4. Discussion

In this study, we combined scRNAseq and bulkRNAseq data to identify the primary mononuclear macrophage subgroups involved in antibody-mediated rejection after kidney transplantation. Additionally, we conducted a thorough investigation of the significant macrophage infiltration observed in ABMR. The specific novel findings demonstrated in this report include the following: 1. In antibody-mediated rejection tissues, M1-like macrophages demonstrate a more pronounced infiltration tendency compared to M2-like macrophages. The degree of this infiltration is intricately linked to the severity of the pathological damage. 2. M1-like macrophages exhibit characteristics of infiltrating cells, while M2-like macrophages display traits of resident cells. These cells originate from the recipient's circulating monocytes and the donor's renal resident macrophages, respectively, and exhibit the potential for mutual transformation. 3. MIF serves as a crucial mediator in the interaction between M1-like infiltrating macrophages, lymphocytes, and vascular endothelial cells. 4. STAT1 is a key transcription factor that regulates the gene expression of M1-like infiltrating macrophages and facilitates the transformation of monocytes into these macrophages. 5. The infiltration of M1-like infiltrating macrophages indicates poor graft prognosis, with the IFNγ pathway playing a central role in these adverse outcomes. 6. Prognosis models utilizing upstream and downstream genes of STAT1 demonstrates robust predictive capabilities. 7.The TLR4-STAT1-PARP9 axis in M1-like infiltrating macrophages may promote the transcription of IFNγ-related genes by inhibiting the ADP-ribosylation of STAT1. Our study provides a new insight into the macrophages clustering and underlying mechanism in ABMR, and provides fresh perspectives on mitigating the pathological lesions of ABMR and enhancing the survival of renal grafts.

Macrophages are typically classified into two groups based on activators (IFNγ or IL-4), namely M1 macrophages (classic macrophages) and M2 macrophages (alternative macrophages) [40]. This rough classification does not fully capture the complex functional phenotypes of macrophages in diverse diseases, but it's role in various disease processes can be mainly concluded into two opposite functional states: proinflammatory and anti-inflammatory. In this study, we identified M1-like and M2-like macrophages within biopsy samples of renal grafts, characterized by high expression of pro-inflammatory and anti-inflammatory genes, respectively. Previous research on ABMR predominantly focused on M2 macrophages [11] due to their critical role in transplant glomerulopathy (TG) [41] and interstitial fibrosis and tubular atrophy (IF/TA) [42]. However, our findings reveal that the infiltration of M1-like macrophages in ABMR is more significant, with higher levels of infiltration correlating with increased Banff lesion scores and poorer graft survival outcomes. Although M2-like macrophages exhibits the anti-inflammatory transcriptomic features typical of traditional M2-type macrophages, their increased infiltration does not distinctly mitigate graft injury. Contrarily, it appears to hasten graft loss. This may be linked to their reparative functions through endothelial-mesenchymal transition and angiogenesis, which paradoxically accelerate renal graft fibrosis. This is consistent with the opinion of Toki et al. [43] that the infiltration of M2 macrophages aggravates renal tubular injury and fibrosis in the transplanted kidneys.

A unique feature of macrophages in allografts is that the donor's macrophages, migrating along with the transplanted organ, become tissue-resident macrophages that participate in inflammation resolution and fibrosis processes. In response to inflammation or

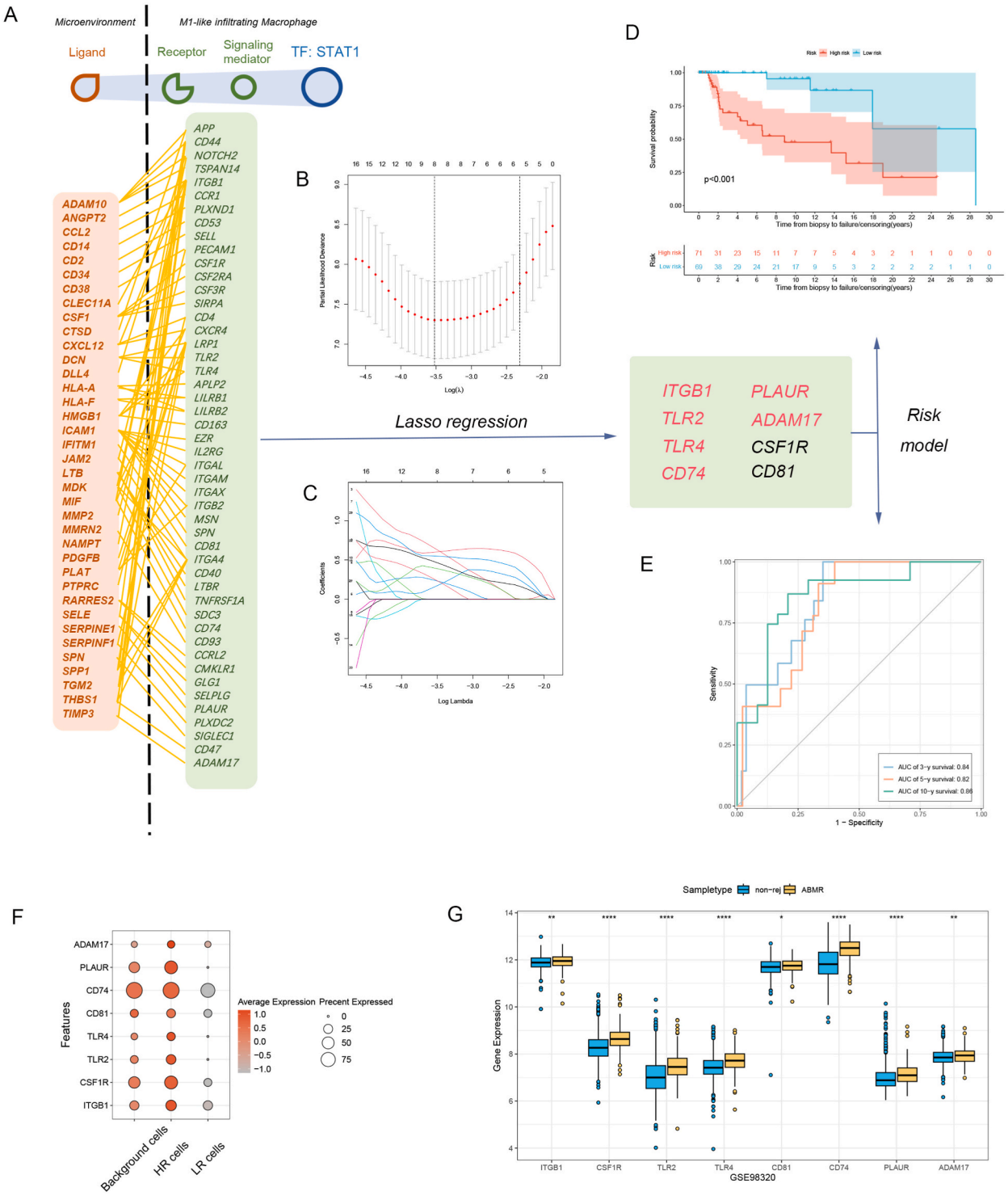

(caption on next page)

Fig. 7. Development and Evaluation of a Prognostic Prediction Model Based on Upstream Genes of STAT1. (A) Schematic representation of the process for constructing the prognostic risk model. The left boxes show the upstream genes of STAT1 (including receptors and signaling mediators) and their paired ligands. The right box indicates the critical upstream genes (PUGs) identified through Cox and Lasso regression analysis. Genes highlighted in red are those with roles in kidney transplantation as confirmed by published literature. (B) Lasso coefficient profiles of the model. (C) Graph depicting the partial likelihood deviance for model optimization. (D) Kaplan-Meier (K–M) survival curve comparing graft survival between high-risk and low-risk groups in the training set. (E) Receiver operating characteristic (ROC) curve for the model, showing the area under the curve (AUC) for 3-year, 5-year, and 10-year graft survival predictions in the training set. (F) Dot plot representing the average expression of critical PUGs (cPUGs) across different prognostic states. (G) cPUGs' expression in ABMR versus non-rejection samples using dataset GSE98320.

damage within the allograft, monocyte-derived macrophages from the recipient are then recruited [44]. Our study confirms this notion and identifies two differentiation trajectories: S100A + monocytes transitioning into M1-like infiltrating macrophages, and TREM2+ resident macrophages evolving into M2-like resident macrophages. These differentiation pathways are informed by the biological properties of monocytes and findings by Kawakami [45], which suggest that most tissue-resident macrophages, including those in renal tissues, predominantly display an M2 macrophage phenotype. FCGR3A + infiltrating macrophages and NR4As + infiltrating macrophages represent intermediate states during differentiation. These two cell types bear resemblance to M1-like infiltrating macrophages and M2-like resident macrophages, respectively, both in terms of their differentiation trajectories and transcriptomic characteristics. Previous studies suggested that the functional Fc gamma receptor (FcγR) IIIA polymorphism FCGR3A-V/F158 on the surface of monocyte/macrophage is in involved in the microcirculatory inflammation caused by DSA [46,47]. Macrophage NR4A1-3 receptors can integrate as well as limit inflammatory signaling, and promote tissue repair [48]. The deletion of NR4A1 can exacerbate the macrophage-mediated kidney injury [49]. It's worth noting that only certain macrophage subsets were identified in the external ABMR samples. These subsets, characterized by marker genes consistent with M1-like infiltrating macrophages, M2-like resident macrophages, and FCGR3A + infiltrating macrophages, indicate that these three subpopulations are conserved in ABMR. Meanwhile, the remaining subsets may exist in an intermediate state of differentiation or under inflammatory stimulation. Fig. 10 illustrates the dynamic transformation pathways among macrophage subsets in ABMR.

MIF is a pleiotropic molecule named for its inhibition of random migration of macrophages [50]. It functions as a pro-inflammatory factor and chemokine, regulating cell proliferation, angiogenesis, and fibrosis [51]. MIF plays a vital role in immune responses; it can recruit macrophages, enhance the expression of HLA-DR on macrophage surfaces, stimulate macrophages through nitric oxide (NO) production, and regulate the proliferation and activation of T cells [52–54]. In acute kidney transplant rejection, the production of local MIF is significantly increased [55], and MIF levels in urine have proven useful for monitoring allogeneic rejection in kidney transplant recipients [56]. D74 is a receptor for extracellular MIF. Upon MIF binding to CD74, it activates the $CD74^{-}$CD44 or CD74-CXCRx signaling complexes [52]. The former activates the ERK pathway [57], influencing cell proliferation and activation [58], while the latter functions in chemotaxis [51]. It has been observed that CD74 is highly expressed in renal tubular epithelium during acute rejection [59]. Our study reveals that MIF acts as a crucial signaling molecule between M1-like infiltrating macrophages, lymphocytes, and endothelial cells, a pattern more prevalent in ABMR. M1-like infiltrating macrophages release MIF to recruit lymphocytes, which in turn activate macrophages via the MIF-CD74 signaling, leading to the production of inflammatory cytokines and consequent endothelial inflammation. However, the deletion of MIF fails to prevent the occurrence of kidney transplant rejection in mice, suggesting that the role of MIF in rejection may be replaced by other molecules [60].

The cytokine IFNγ derived from type 1 helper T cells (Th1) binds to the IFN receptor on the cell surface, then activates the Janus kinase (JAK)-signal transducer and the downstream STAT1 pathway. This activation induces the expression of interferon-stimulated genes (ISGs) that play a critical role in immune effector functions, thereby influencing tissue homeostasis, inflammation, and immune responses [61]. Previous studies have shown that free or intracellular IFNγ is associated with acute rejection after kidney transplantation [62] and serves as a biomarker for the detection of acute rejection [63]. However, the mechanism is not elucidated. Zhang et al. [64] suggested IFN-γ as a determinant of ABMR and clinical outcomes in patients after kidney transplantation. Our study believed that M1-like infiltrating macrophages expressed a large number of IFNγ-induced transcripts with STAT1 as the core of the gene regulatory network after receiving IFNγ signal, which may aggravate tissue damage in AMBR. Likewise, Callemeyn et al. [65] discovered that biopsy specimens with ABMR histology showed overexpression of transcripts mostly related to IFNγ-induced pathways. Furthermore, the prognosis model built with upstream and downstream genes of STAT1 demonstrates strong predictive capabilities. These genes are implicated in various renal conditions, such as ischemia-reperfusion (ITGB1 [66], TLR2/4 [67,68]), acute and chronic rejection (TLR4 [69], HLA-E [70,71], PSMB8 [72]), recurrent primary nephropathy (PLAUR [73]), metabolic diseases associated with renal transplants (ADAM17 [74]), and serve as non-invasive molecular markers for ABMR diagnosis (GBP1 [75,76]), and apoptosis processes (TNFSF10 [77]).

Significantly, our research succeeded in identifying a novel prognostic molecule, PARP9, whose role in kidney transplantation remains largely unexplored. Functioning as a downstream molecule of STAT1, PARP9 appears to be pivotal in the phenotypic transformation of pro-inflammatory macrophages and in amplifying IFNγ-induced gene expression. Previous studies have revealed that silencing PARP9 can suppress the expression of pro-inflammatory genes and the IFNγ-induced phosphorylation of STAT1 in macrophages [39]. The PARP9-DTX3L complex interacts with STAT1 and activates E3 ubiquitinase to enhances the expression of interferon-stimulated genes [78]. The Poly-ADP-ribose polymerase (PARP) family constitutes a group of mammalian ADP-ribosyltransferases (ARTs) that catalyze the transfer of ADP-ribose from NAD + to various substrates, resulting in ADP-ribosylation [79]. This process represents a post-translational modification that regulates proteins, nucleic acids, and metabolites. Although part of the PARP family, PARP9 lacks transferase activity [80]. Intriguingly, the macrodomain1 of PARP9 exhibits hydrolytic activity, acting as an 'eraser' in the realm of epigenetics [81]. This function is crucial for regulating ADPr levels in other transferases or

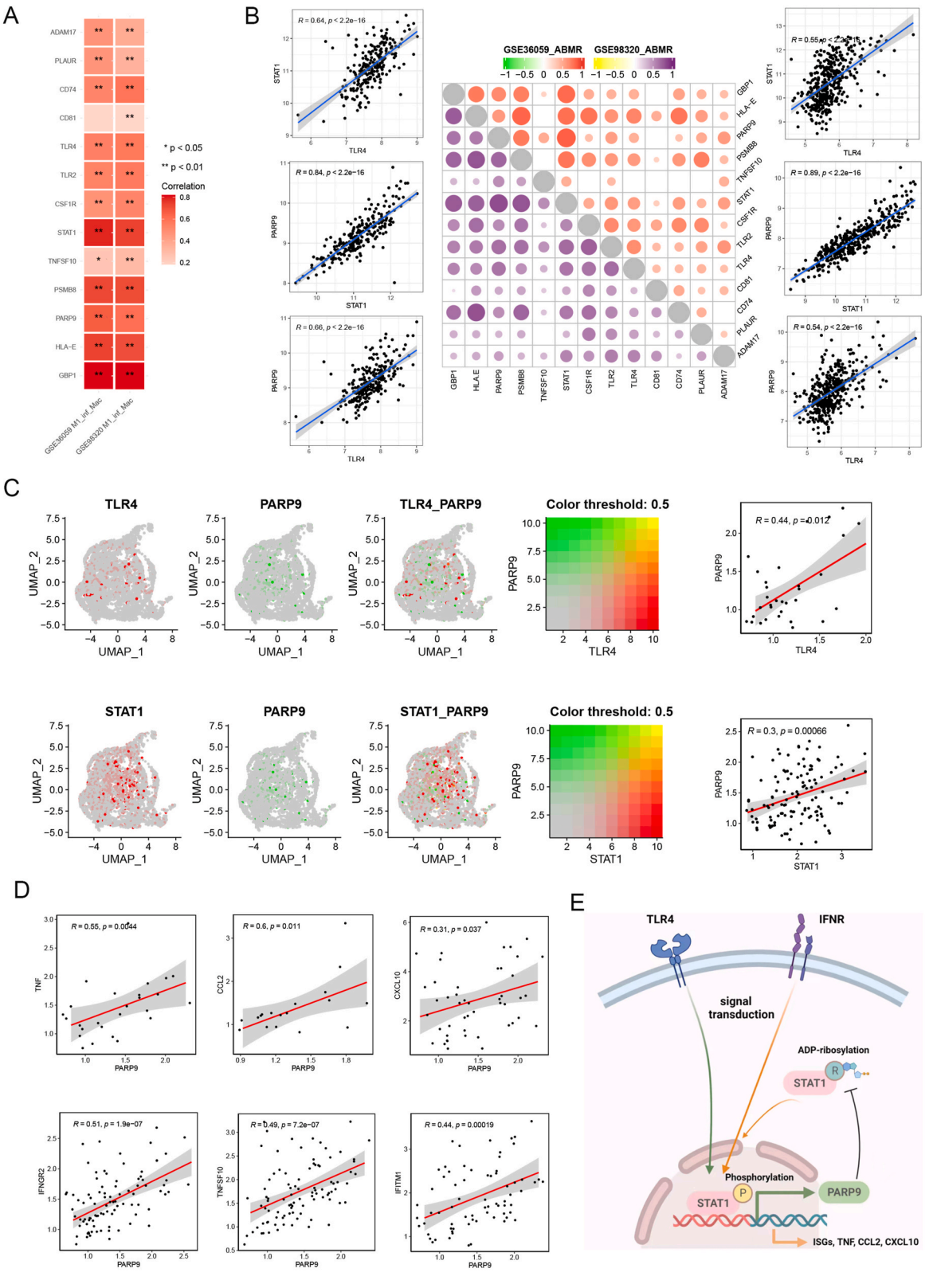

(caption on next page)

Fig. 8. Analysis of Correlations Between STAT1 and Its Upstream and Downstream Genes. (A) Heatmap showing the correlation between STAT1-up/downstream genes and infiltration of M1-like infiltrating macrophages in GSE36059 and GSE98320. (B) Analysis of the correlations between STAT1 upstream/downstream genes in GSE36059 (upper right) and GSE98320 (upper left). Scatter plots detail specific correlation coefficients and p-values for selected gene pairs. (C) UMAP exhibiting coordinated expression of TLR4/STAT1 and PARP9 of M1-like infiltrating macrophages in ABMR. Accompanying scatter plots show the correlation between TLR4/STAT1 and PARP9. (D) Scatter plots of correlation between PARP9 and pro-inflammatory genes (TNF, CCL2, and CXCL10), IFNγ receptor gene (IFNR2), and IFNγ stimulated genes (TNFSF10 and IFITM1). (E) Potential mechanism of TLR4-STAT1-PARP9 axis of M1-like infiltrating macrophages in ABMR.

under specific cellular contexts. This supports the explanation of the experimental phenomenon by Hiroshi et al. [39]: the opposing pro-inflammatory and anti-inflammatory phenotypes in macrophages driven by PARP9 and PARP14 might result from PARP9 inhibiting the ADP-ribosylation of STAT1 by PARP14. In our research, STAT1 serves as the intersection of TLR4 and IFNγ signaling crosstalk. PARP9 enhances the phosphorylation of STAT1 by modulating its ADP-ribosylation, leading to increased IFNγ-induced genes expression. This positive feedback loop intensifies the pro-inflammatory phenotypic polarization of M1-like macrophages, contributing to their pro-inflammatory impact in ABMR. Consequently, targeting PARP9 could be a promising therapeutic strategy for ABMR.

Nevertheless, our research faces certain limitations: 1. Due to the complexity and high costs of single-cell sequencing technology, our study includes a relatively small sample size. Additionally, The ABMR cases included in the study exhibit at leat some differences in pathological mechanisms, and the different types of antibody and donor-recipient mismatches are not taken into account. Thus, these factors introduced potential confounding variables. 2. The number of immune cells obtained by single-cell technology and the depth of sequencing are limited, and some macrophages may be lost or physically activated in the process of cell dissociation [82], which brings disturbance to data analysis. 3. Bioinformatics analysis can determine correlations between molecules but struggles to establish causality. Hence, our study's proposed mechanisms necessitate further validation via knockout and overexpression experiments. Nonetheless, our findings are enlightening, paving the way for future research on ABMR-associated macrophages.

5. Conclusion

In conclusion, this study depicted the macrophage profile in antibody-mediated rejection after kidney transplantation by combining scRNA-seq and bulkRNA-seq data, highlighted the negative impact of M1-like infiltrating macrophages on graft injury and prognosis, and found that PARP9 may be a therapeutic target for alleviating inflammatory damage in ABMR.

Funding

This work was supported by Social Livelihood Field Science and Technology project of Bishan District Science and Technology Bureau (BSKJ2022018).

Data availability statement

The datasets presented in this study can be found in online repositories. The names of the repository/repositories and accession number(s) can be found in the article/Supplementary Material.

CRediT authorship contribution statement

Qidan Pang: Writing – original draft, Formal analysis, Conceptualization. **Liang Chen:** Formal analysis, Data curation. **Changyong An:** Writing – review & editing, Data curation. **Juan Zhou:** Writing – original draft, Data curation. **Hanyu Xiao:** Writing – review & editing, Methodology, Conceptualization.

Declaration of generative AI and AI-assisted technologies in the writing process

During the preparation of this work the author(s) used ChatGPT 4.0 in order to improve readability and language. After using this tool/service, the authors reviewed and edited the content as needed and take full responsibility for the content of the publication.

Declaration of competing interest

The authors declare that they have no known competing financial interests or personal relationships that could have appeared to influence the work reported in this paper.

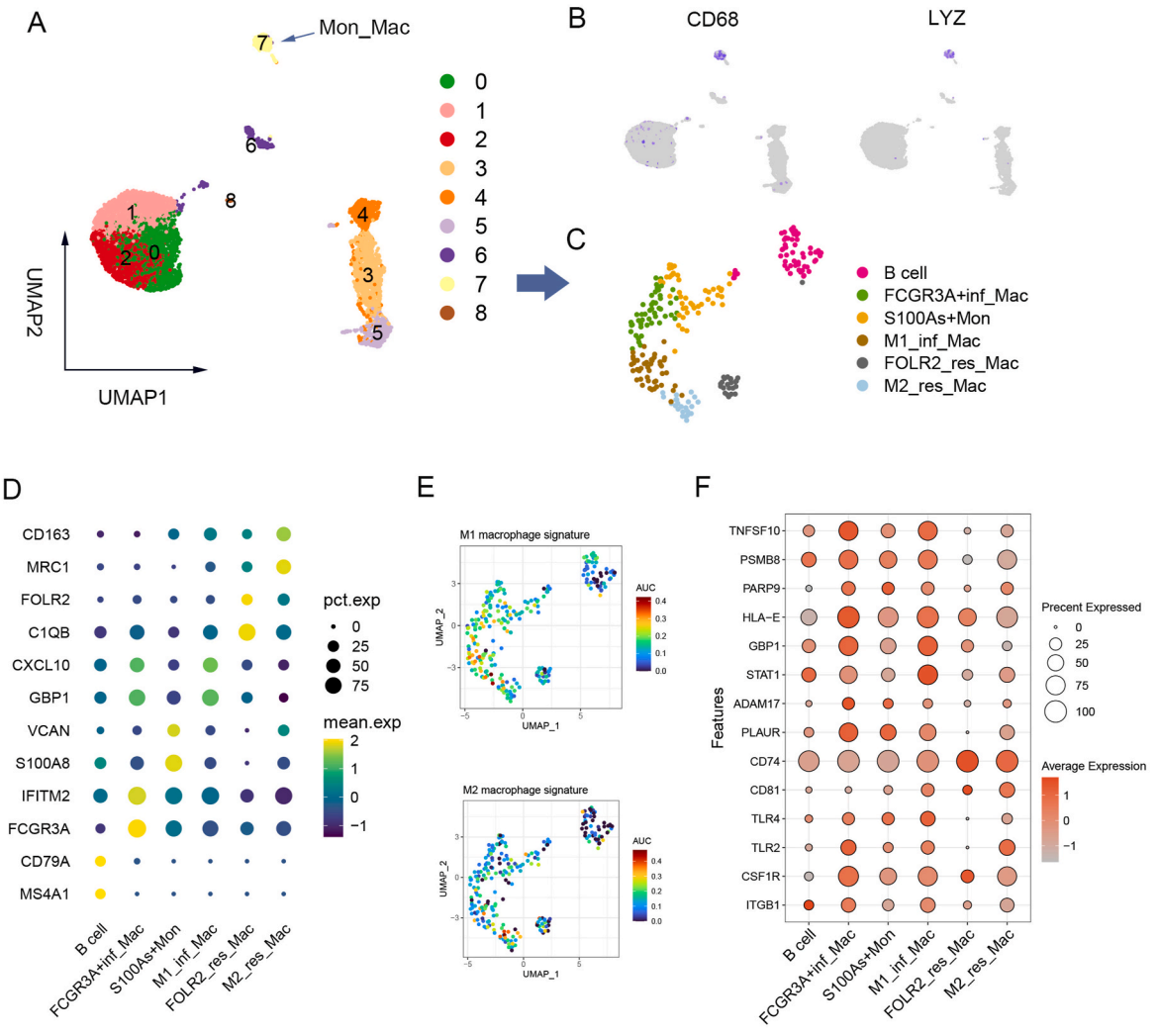

(caption on next page)

Fig. 9. Validation of Study Findings Using an Independent External Single-Cell Dataset. (A) UMAP of 9 distinct cell clusters identified in the dataset. (B) UMAP showing distribution and expression of mon-macrophage related marker genes (CD68 and LYZ). (C) Re-clustering of mon-macrophage clusters. (D) Dotplot detailing the expression of specific marker genes for each monocyte-macrophage subcluster. (E) UMAPs demonstrating the area under curve (AUC) values and distribution of macrophage-related phenotypic signatures in the subclusters. (F) Dot plot presenting the expression patterns of STAT1 upstream/downstream genes in the subclusters. UMAP exhibiting coordinated expression of TLR4 (G)/STAT1 (H) and PARP9 of M1-like infiltrating macrophages in ABMR. Accompanying scatter plots illustrate the correlations between TLR4 (G)/STAT1 (H) and PARP9.

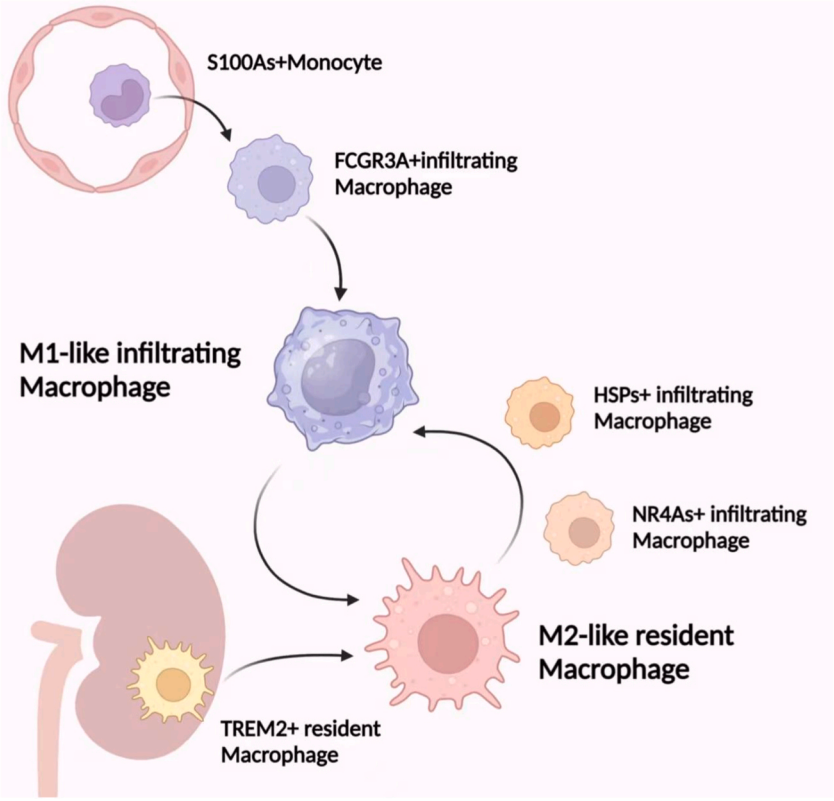

Fig. 10. Transformation Pathways Among Macrophage Subsets in ABMR. M1-like infiltrating macrophages originate from S100As + monocytes in the recipient's circulation, transitioning through an intermediate FCGR3A + infiltrating macrophage state. Meanwhile, M2-like resident macrophages differentiate from donor renal tissue resident cells, specifically TREM2+ resident macrophages. Additionally, M1-like and M2-like macrophages can interconvert through two transitional states: NR4As+ and HSPs + infiltrating macrophages.

Acknowledgements

Not applicable.

Appendix A. Supplementary data

Supplementary data to this article can be found online at https://doi.org/10.1016/j.heliyon.2024.e27865.

References

[1] J. Callemeyn, B. Lamarthee, A. Koenig, P. Koshy, O. Thaunat, M. Naesens, Allorecognition and the spectrum of kidney transplant rejection, Kidney Int. 101 (2022) 692–710.
[2] K.L. Lentine, J.M. Smith, J.M. Miller, K. Bradbrook, L. Larkin, S. Weiss, D.K. Handarova, K. Temple, A.K. Israni, J.J. Snyder, OPTN/SRTR 2021 annual data report: kidney, Am. J. Transplant. 23 (2023) S21–S120.
[3] A. Loupy, C. Lefaucheur, Antibody-mediated rejection of solid-organ allografts, N. Engl. J. Med. 379 (2018) 1150–1160.
[4] M. Haas, The relationship between pathologic lesions of active and chronic antibody-mediated rejection in renal allografts, Am. J. Transplant. 18 (2018) 2849–2856.

[5] K. Lackner, S. Ebner, K. Watschinger, M. Maglione, Multiple shades of gray-macrophages in acute allograft rejection, Int. J. Mol. Sci. 24 (2023).
[6] K.J. Tinckam, O. Djurdjev, A.B. Magil, Glomerular monocytes predict worse outcomes after acute renal allograft rejection independent of C4d status, Kidney Int. 68 (2005) 1866–1874.
[7] J.H. Brasen, A. Khalifa, J. Schmitz, W. Dai, G. Einecke, A. Schwarz, M. Hallensleben, B. Schmidt, H.H. Kreipe, H. Haller, S. von Vietinghoff, Macrophage density in early surveillance biopsies predicts future renal transplant function, Kidney Int. 92 (2017) 479–489.
[8] T. Bergler, B. Jung, F. Bourier, L. Kuhne, M.C. Banas, P. Rummele, S. Wurm, B. Banas, Infiltration of macrophages correlates with severity of allograft rejection and outcome in human kidney transplantation, PLoS One 11 (2016) e0156900.
[9] M.J. Raftery, D. Seron, G. Koffman, B. Hartley, G. Janossy, J.S. Cameron, The relevance of induced class II HLA antigens and macrophage infiltration in early renal allograft biopsies, Transplantation 48 (1989) 238–243.
[10] S.E. Panzer, Macrophages in transplantation: a matter of plasticity, polarization, and diversity, Transplantation 106 (2022) 257–267.
[11] A.F. Malone, Monocytes and macrophages in kidney transplantation and insights from single cell RNA-seq studies, Kidney 2 (2021) 1654–1659.
[12] F. Schreibing, R. Kramann, Mapping the human kidney using single-cell genomics, Nat. Rev. Nephrol. 18 (2022) 347–360.
[13] H. Wu, A.F. Malone, E.L. Donnelly, Y. Kirita, K. Uchimura, S.M. Ramakrishnan, J.P. Gaut, B.D. Humphreys, Single-cell transcriptomics of a human kidney allograft biopsy specimen defines a diverse inflammatory response, J. Am. Soc. Nephrol. 29 (2018) 2069–2080.
[14] A.F. Malone, H. Wu, C. Fronick, R. Fulton, J.P. Gaut, B.D. Humphreys, Harnessing expressed single nucleotide variation and single cell RNA sequencing to define immune cell chimerism in the rejecting kidney transplant, J. Am. Soc. Nephrol. 31 (2020) 1977–1986.
[15] S. Cormican, N. Negi, S.D. Naicker, M.N. Islam, B. Fazekas, R. Power, T.P. Griffin, M.C. Dennedy, B. MacNeill, A.F. Malone, M.D. Griffin, Chronic kidney disease is characterized by expansion of a distinct proinflammatory intermediate monocyte subtype and by increased monocyte adhesion to endothelial cells, J. Am. Soc. Nephrol. 34 (2023) 793–808.
[16] B. Lamarthee, J. Callemeyn, Y. Van Herck, A. Antoranz, D. Anglicheau, P. Boada, J.U. Becker, T. Debyser, F. De Smet, K. De Vusser, M. Eloudzeri, A. Franken, W. Gwinner, P. Koshy, D. Kuypers, D. Lambrechts, P. Marquet, V. Mathias, M. Rabant, M.M. Sarwal, A. Senev, T.K. Sigdel, B. Sprangers, O. Thaunat, C. Tinel, T. Van Brussel, A. Van Craenenbroeck, E. Van Loon, T. Vaulet, F. Bosisio, M. Naesens, Transcriptional and spatial profiling of the kidney allograft unravels a central role for FcγRIII+ innate immune cells in rejection, Nat. Commun. 14 (2023) 4359.
[17] J. Reeve, J. Sellares, M. Mengel, B. Sis, A. Skene, L. Hidalgo, D.G. de Freitas, K.S. Famulski, P.F. Halloran, Molecular diagnosis of T cell-mediated rejection in human kidney transplant biopsies, Am. J. Transplant. 13 (2013) 645–655.
[18] J. Reeve, G.A. Bohmig, F. Eskandary, G. Einecke, C. Lefaucheur, A. Loupy, P.F. Halloran, Assessing rejection-related disease in kidney transplant biopsies based on archetypal analysis of molecular phenotypes, JCI Insight (2017) 2.
[19] G. Einecke, J. Reeve, B. Sis, M. Mengel, L. Hidalgo, K.S. Famulski, A. Matas, B. Kasiske, B. Kaplan, P.F. Halloran, A molecular classifier for predicting future graft loss in late kidney transplant biopsies, J. Clin. Invest. 120 (2010) 1862–1872.
[20] C. Hu, T. Li, Y. Xu, X. Zhang, F. Li, J. Bai, J. Chen, W. Jiang, K. Yang, Q. Ou, X. Li, P. Wang, Y. Zhang, CellMarker 2.0: an updated database of manually curated cell markers in human/mouse and web tools based on scRNA-seq data, Nucleic Acids Res. 51 (2023) D870–D876.
[21] B.J. Stewart, J.R. Ferdinand, M.D. Young, T.J. Mitchell, K.W. Loudon, A.M. Riding, N. Richoz, G.L. Frazer, J. Staniforth, B.F. Vieira, R.A. Botting, D.M. Popescu, R. Vento-Tormo, E. Stephenson, A. Cagan, S.J. Farndon, K. Polanski, M. Efremova, K. Green, C.V.M. Del, C. Guzzo, G. Collord, L. Mamanova, T. Aho, J. N. Armitage, A. Riddick, I. Mushtaq, S. Farrell, D. Rampling, J. Nicholson, A. Filby, J. Burge, S. Lisgo, S. Lindsay, M. Bajenoff, A.Y. Warren, G.D. Stewart, N. Sebire, N. Coleman, M. Haniffa, S.A. Teichmann, S. Behjati, M.R. Clatworthy, Spatiotemporal immune zonation of the human kidney, Science 365 (2019) 1461–1466.
[22] L. Zheng, S. Qin, W. Si, A. Wang, B. Xing, R. Gao, X. Ren, L. Wang, X. Wu, J. Zhang, N. Wu, N. Zhang, H. Zheng, H. Ouyang, K. Chen, Z. Bu, X. Hu, J. Ji, Z. Zhang, Pan-cancer single-cell landscape of tumor-infiltrating T cells, Science 374 (2021) abe6474.
[23] K. Jin, S. Gao, P. Yang, R. Guo, D. Li, Y. Zhang, X. Lu, G. Fan, X. Fan, Single-cell RNA sequencing reveals the temporal diversity and dynamics of cardiac immunity after myocardial infarction, Small Methods 6 (2022) e2100752.
[24] K.A. Zimmerman, M.R. Bentley, J.M. Lever, Z. Li, D.K. Crossman, C.J. Song, S. Liu, M.R. Crowley, J.F. George, M. Mrug, B.K. Yoder, Single-cell RNA sequencing identifies candidate renal resident macrophage gene expression signatures across species, J. Am. Soc. Nephrol. 30 (2019) 767–781.
[25] S. Chen, A. Saeed, Q. Liu, Q. Jiang, H. Xu, G.G. Xiao, L. Rao, Y. Duo, Macrophages in immunoregulation and therapeutics, Signal Transduct. Targeted Ther. 8 (2023) 207.
[26] J. Chen, E.E. Bardes, B.J. Aronow, A.G. Jegga, ToppGene Suite for gene list enrichment analysis and candidate gene prioritization, Nucleic Acids Res. 37 (2009) W305–W311.
[27] A.M. Newman, C.B. Steen, C.L. Liu, A.J. Gentles, A.A. Chaudhuri, F. Scherer, M.S. Khodadoust, M.S. Esfahani, B.A. Luca, D. Steiner, M. Diehn, A.A. Alizadeh, Determining cell type abundance and expression from bulk tissues with digital cytometry, Nat. Biotechnol. 37 (2019) 773–782.
[28] A. Loupy, M. Mengel, M. Haas, Thirty years of the International Banff Classification for Allograft Pathology: the past, present, and future of kidney transplant diagnostics, Kidney Int. 101 (2022) 678–691.
[29] S. Jin, C.F. Guerrero-Juarez, L. Zhang, I. Chang, R. Ramos, C.H. Kuan, P. Myung, M.V. Plikus, Q. Nie, Inference and analysis of cell-cell communication using CellChat, Nat. Commun. 12 (2021) 1088.
[30] M. Efremova, M. Vento-Tormo, S.A. Teichmann, R. Vento-Tormo, CellPhoneDB: inferring cell-cell communication from combined expression of multi-subunit ligand-receptor complexes, Nat. Protoc. 15 (2020) 1484–1506.
[31] S. Aibar, C.B. Gonzalez-Blas, T. Moerman, V.A. Huynh-Thu, H. Imrichova, G. Hulselmans, F. Rambow, J.C. Marine, P. Geurts, J. Aerts, J. van den Oord, Z. K. Atak, J. Wouters, S. Aerts, SCENIC: single-cell regulatory network inference and clustering, Nat. Methods 14 (2017) 1083–1086.
[32] J. Cao, M. Spielmann, X. Qiu, X. Huang, D.M. Ibrahim, A.J. Hill, F. Zhang, S. Mundlos, L. Christiansen, F.J. Steemers, C. Trapnell, J. Shendure, The single-cell transcriptional landscape of mammalian organogenesis, Nature 566 (2019) 496–502.
[33] X. Qiu, Q. Mao, Y. Tang, L. Wang, R. Chawla, H.A. Pliner, C. Trapnell, Reversed graph embedding resolves complex single-cell trajectories, Nat. Methods 14 (2017) 979–982.
[34] D. Sun, X. Guan, A.E. Moran, L.Y. Wu, D.Z. Qian, P. Schedin, M.S. Dai, A.V. Danilov, J.J. Alumkal, A.C. Adey, P.T. Spellman, Z. Xia, Identifying phenotype-associated subpopulations by integrating bulk and single-cell sequencing data, Nat. Biotechnol. 40 (2022) 527–538.
[35] S. Morabito, F. Reese, N. Rahimzadeh, E. Miyoshi, V. Swarup, hdWGCNA identifies co-expression networks in high-dimensional transcriptomics data, Cell Rep Methods 3 (2023) 100498.
[36] R. Janky, A. Verfaillie, H. Imrichova, B. Van de Sande, L. Standaert, V. Christiaens, G. Hulselmans, K. Herten, S.M. Naval, D. Potier, D. Svetlichnyy, A. Z. Kalender, M. Fiers, J.C. Marine, S. Aerts, iRegulon: from a gene list to a gene regulatory network using large motif and track collections, PLoS Comput. Biol. 10 (2014) e1003731.
[37] R. Browaeys, W. Saelens, Y. Saeys, NicheNet: modeling intercellular communication by linking ligands to target genes, Nat. Methods 17 (2020) 159–162.
[38] H. Iwata, C. Goettsch, A. Sharma, P. Ricchiuto, W.W. Goh, A. Halu, I. Yamada, H. Yoshida, T. Hara, M. Wei, N. Inoue, D. Fukuda, A. Mojcher, P.C. Mattson, A. L. Barabasi, M. Boothby, E. Aikawa, S.A. Singh, M. Aikawa, PARP9 and PARP14 cross-regulate macrophage activation via STAT1 ADP-ribosylation, Nat. Commun. 7 (2016) 12849.
[39] K. Sikorski, A. Czerwoniec, J.M. Bujnicki, J. Wesoly, H.A. Bluyssen, STAT1 as a novel therapeutical target in pro-atherogenic signal integration of IFNgamma, TLR4 and IL-6 in vascular disease, Cytokine Growth Factor Rev. 22 (2011) 211–219.
[40] C.D. Mills, K. Kincaid, J.M. Alt, M.J. Heilman, A.M. Hill, M-1/M-2 macrophages and the Th1/Th2 paradigm, J. Immunol. 164 (2000) 6166–6173.
[41] J. Kim, S.E. Choi, B.J. Lim, Y.S. Kim, K.H. Huh, J. Lee, S.I. Kim, M.S. Kim, H.J. Jeong, Clinical significance of macrophage polarization in antibody-mediated rejection of renal allograft, Transplant. Proc. 50 (2018) 1005–1008.
[42] C. Wu, Y. Zhao, X. Xiao, Y. Fan, M. Kloc, W. Liu, R.M. Ghobrial, P. Lan, X. He, X.C. Li, Graft-infiltrating macrophages adopt an M2 phenotype and are inhibited by purinergic receptor P2X7 antagonist in chronic rejection, Am. J. Transplant. 16 (2016) 2563–2573.

[43] D. Toki, W. Zhang, K.L. Hor, D. Liuwantara, S.I. Alexander, Z. Yi, R. Sharma, J.R. Chapman, B.J. Nankivell, B. Murphy, P.J. O'Connell, The role of macrophages in the development of human renal allograft fibrosis in the first year after transplantation, Am. J. Transplant. 14 (2014) 2126–2136.
[44] V. Grau, B. Herbst, B. Steiniger, Dynamics of monocytes/macrophages and T lymphocytes in acutely rejecting rat renal allografts, Cell Tissue Res. 291 (1998) 117–126.
[45] T. Kawakami, J. Lichtnekert, L.J. Thompson, P. Karna, H. Bouabe, T.M. Hohl, J.W. Heinecke, S.F. Ziegler, P.J. Nelson, J.S. Duffield, Resident renal mononuclear phagocytes comprise five discrete populations with distinct phenotypes and functions, J. Immunol. 191 (2013) 3358–3372.
[46] M.L. Arnold, A. Kainz, L.G. Hidalgo, F. Eskandary, N. Kozakowski, M. Wahrmann, H. Haslacher, R. Oberbauer, A. Heilos, B.M. Spriewald, P.F. Halloran, G. A. Bohmig, Functional Fc gamma receptor gene polymorphisms and donor-specific antibody-triggered microcirculation inflammation, Am. J. Transplant. 18 (2018) 2261–2273.
[47] N. Litjens, A. Peeters, J.K. Gestel, M. Klepper, M. Betjes, The FCGR3A 158 V/V-genotype is associated with decreased survival of renal allografts with chronic active antibody-mediated rejection, Sci. Rep. 11 (2021) 7903.
[48] E.P. Murphy, D. Crean, Molecular interactions between NR4A orphan nuclear receptors and NF-kappaB are required for appropriate inflammatory responses and immune cell homeostasis, Biomolecules 5 (2015) 1302–1318.
[49] L. Westbrook, A.C. Johnson, K.R. Regner, J.M. Williams, D.L. Mattson, P.B. Kyle, J.R. Henegar, M.R. Garrett, Genetic susceptibility and loss of Nr4a1 enhances macrophage-mediated renal injury in CKD, J. Am. Soc. Nephrol. 25 (2014) 2499–2510.
[50] J. Bernhagen, R. Krohn, H. Lue, J.L. Gregory, A. Zernecke, R.R. Koenen, M. Dewor, I. Georgiev, A. Schober, L. Leng, T. Kooistra, G. Fingerle-Rowson, P. Ghezzi, R. Kleemann, S.R. McColl, R. Bucala, M.J. Hickey, C. Weber, MIF is a noncognate ligand of CXC chemokine receptors in inflammatory and atherogenic cell recruitment, Nat. Med. 13 (2007) 587–596.
[51] M.D. Sanchez-Nino, A.B. Sanz, O. Ruiz-Andres, J. Poveda, M.C. Izquierdo, R. Selgas, J. Egido, A. Ortiz, MIF, CD74 and other partners in kidney disease: tales of a promiscuous couple, Cytokine Growth Factor Rev. 24 (2013) 23–40.
[52] M.J. Herriott, H. Jiang, C.A. Stewart, D.J. Fast, R.W. Leu, Mechanistic differences between migration inhibitory factor (MIF) and IFN-gamma for macrophage activation. MIF and IFN-gamma synergize with lipid A to mediate migration inhibition but only IFN-gamma induces production of TNF-alpha and nitric oxide, J. Immunol. 150 (1993) 4524–4531.
[53] T. Calandra, L.A. Spiegel, C.N. Metz, R. Bucala, Macrophage migration inhibitory factor is a critical mediator of the activation of immune cells by exotoxins of Gram-positive bacteria, Proc. Natl. Acad. Sci. U.S.A. 95 (1998) 11383–11388.
[54] M. Bacher, C.N. Metz, T. Calandra, K. Mayer, J. Chesney, M. Lohoff, D. Gemsa, T. Donnelly, R. Bucala, An essential regulatory role for macrophage migration inhibitory factor in T-cell activation, Proc. Natl. Acad. Sci. U.S.A. 93 (1996) 7849–7854.
[55] F.G. Brown, D.J. Nikolic-Paterson, C. Metz, R. Bucala, R.C. Atkins, H.Y. Lan, Up-regulation of macrophage migration inhibitory factor in acute renal allograft rejection in the rat, Clin. Exp. Immunol. 118 (1999) 329–336.
[56] F.G. Brown, D.J. Nikolic-Paterson, S.J. Chadban, J. Dowling, M. Jose, C.N. Metz, R. Bucala, R.C. Atkins, Urine macrophage migration inhibitory factor concentrations as a diagnostic tool in human renal allograft rejection, Transplantation 71 (2001) 1777–1783.
[57] H. Liao, R. Bucala, R.A. Mitchell, Adhesion-dependent signaling by macrophage migration inhibitory factor (MIF), J. Biol. Chem. 278 (2003) 76–81.
[58] R.A. Mitchell, C.N. Metz, T. Peng, R. Bucala, Sustained mitogen-activated protein kinase (MAPK) and cytoplasmic phospholipase A2 activation by macrophage migration inhibitory factor (MIF). Regulatory role in cell proliferation and glucocorticoid action, J. Biol. Chem. 274 (1999) 18100–18106.
[59] M. Saleem, G.J. Sawyer, R.A. Schofield, N.D. Seymour, K. Gustafsson, J.W. Fabre, Discordant expression of major histocompatibility complex class II antigens and invariant chain in interstitial dendritic cells. Implications for self-tolerance and immunity, Transplantation 63 (1997) 1134–1138.
[60] M.D. Jose, J.R. David, R.C. Atkins, S.J. Chadban, Blockade of macrophage migration inhibitory factor does not prevent acute renal allograft rejection, Am. J. Transplant. 3 (2003) 1099–1106.
[61] L.B. Ivashkiv, IFNgamma: signalling, epigenetics and roles in immunity, metabolism, disease and cancer immunotherapy, Nat. Rev. Immunol. 18 (2018) 545–558.
[62] O. Millan, L. Rafael-Valdivia, S.D. San, F. Boix, M.J. Castro-Panete, M. Lopez-Hoyos, M. Muro, D. Valero-Hervas, A. Rimola, M. Navasa, P. Munoz, M. Miras, A. Andres, L. Guirado, J. Pascual, M. Brunet, Should IFN-gamma, IL-17 and IL-2 be considered predictive biomarkers of acute rejection in liver and kidney transplant? Results of a multicentric study, Clin. Immunol. 154 (2014) 141–154.
[63] J. Karczewski, M. Karczewski, K. Wiktorowicz, Pretransplant urine cytokine pattern predicts acute kidney rejection, Cytokine 51 (2010) 10–11.
[64] H. Zhang, D. Zhang, Y. Xu, H. Zhang, Z. Zhang, X. Hu, Interferon-gamma and its response are determinants of antibody-mediated rejection and clinical outcomes in patients after renal transplantation, GENES IMMUN 25 (2024) 66–81.
[65] J. Callemeyn, E. Lerut, H. de Loor, I. Arijs, O. Thaunat, A. Koenig, V. Meas-Yedid, J.C. Olivo-Marin, P. Halloran, J. Chang, L. Thorrez, D. Kuypers, B. Sprangers, L. Van Lommel, F. Schuit, M. Essig, W. Gwinner, D. Anglicheau, P. Marquet, M. Naesens, Transcriptional changes in kidney allografts with histology of antibody-mediated rejection without anti-HLA donor-specific antibodies, J. Am. Soc. Nephrol. 31 (2020) 2168–2183.
[66] Y. Gao, W. Xu, C. Guo, T. Huang, GATA1 regulates the microRNA-328-3p/PIM1 axis via circular RNA ITGB1 to promote renal ischemia/reperfusion injury in HK-2 cells, Int. J. Mol. Med. 50 (2022).
[67] B. Kruger, S. Krick, N. Dhillon, S.M. Lerner, S. Ames, J.S. Bromberg, M. Lin, L. Walsh, J. Vella, M. Fischereder, B.K. Kramer, R.B. Colvin, P.S. Heeger, B. T. Murphy, B. Schroppel, Donor Toll-like receptor 4 contributes to ischemia and reperfusion injury following human kidney transplantation, Proc. Natl. Acad. Sci. U.S.A. 106 (2009) 3390–3395.
[68] M.E. Mohamed, M.A. Elmorsy, N.S. Younis, Renal ischemia/reperfusion mitigation via geraniol: the role of nrf-2/HO-1/NQO-1 and tlr2,4/MYD88/NFkappaB pathway, Antioxidants 11 (2022).
[69] Y.H. Hwang, H. Ro, I. Choi, H. Kim, K.H. Oh, J.I. Hwang, M.H. Park, S. Kim, J. Yang, C. Ahn, Impact of polymorphisms of TLR4/CD14 and TLR3 on acute rejection in kidney transplantation, Transplantation 88 (2009) 699–705.
[70] B.I. Shaw, D.K. Cheng, C.R. Acharya, R.B. Ettenger, H.K. Lyerly, Q. Cheng, A.D. Kirk, E.T. Chambers, An age-independent gene signature for monitoring acute rejection in kidney transplantation, THERANOSTICS 10 (2020) 6977–6986.
[71] B. de Miranda, G.F. Gelmini, M. Risti, V. Hauer, S.J. Da, V. Roxo, M. Bicalho, D. Malheiros, HLA-E genotyping and its relevance in kidney transplantation outcome, HLA 95 (2020) 457–464.
[72] J. Li, M. Basler, G. Alvarez, T. Brunner, C.J. Kirk, M. Groettrup, Immunoproteasome inhibition prevents chronic antibody-mediated allograft rejection in renal transplantation, Kidney Int. 93 (2018) 670–680.
[73] W. Winnicki, G. Sunder-Plassmann, G. Sengolge, A. Handisurya, H. Herkner, C. Kornauth, B. Bielesz, L. Wagner, Z. Kikic, S. Pajenda, T. Reiter, B. Schairer, A. Schmidt, Diagnostic and prognostic value of soluble urokinase-type plasminogen activator receptor (suPAR) in focal segmental glomerulosclerosis and impact of detection method, Sci. Rep. 9 (2019) 13783.
[74] S. Adepu, K. Katta, U.J. Tietge, A.J. Kwakernaak, W. Dam, H. van Goor, R.P. Dullaart, G.J. Navis, S.J. Bakker, J. van den Born, Hepatic syndecan-1 changes associate with dyslipidemia after renal transplantation, Am. J. Transplant. 14 (2014) 2328–2338.
[75] E. Van Loon, S. Gazut, S. Yazdani, E. Lerut, H. de Loor, M. Coemans, L.H. Noel, L. Thorrez, L. Van Lommel, F. Schuit, B. Sprangers, D. Kuypers, M. Essig, W. Gwinner, D. Anglicheau, P. Marquet, M. Naesens, Development and validation of a peripheral blood mRNA assay for the assessment of antibody-mediated kidney allograft rejection: a multicentre, prospective study, EBioMedicine 46 (2019) 463–472.
[76] B. Chauveau, A.A. Raymond, S. Di Tommaso, J. Visentin, A. Vermorel, N. Dugot-Senant, C. Dourthe, J.W. Dupuy, J. Dechanet-Merville, V.H.J. Duong, M. Rabant, L. Couzi, F. Saltel, P. Merville, The proteome of antibody-mediated rejection: from glomerulitis to transplant glomerulopathy, Biomedicines 10 (2022).
[77] Z. Zhao, C. Yang, L. Wang, L. Li, T. Zhao, L. Hu, R. Rong, M. Xu, T. Zhu, The regulatory T cell effector soluble fibrinogen-like protein 2 induces tubular epithelial cell apoptosis in renal transplantation, Exp. Biol. Med. 239 (2014) 193–201.

[78] Y. Zhang, D. Mao, W.T. Roswit, X. Jin, A.C. Patel, D.A. Patel, E. Agapov, Z. Wang, R.M. Tidwell, J.J. Atkinson, G. Huang, R. McCarthy, J. Yu, N.E. Yun, S. Paessler, T.G. Lawson, N.S. Omattage, T.J. Brett, M.J. Holtzman, PARP9-DTX3L ubiquitin ligase targets host histone H2BJ and viral 3C protease to enhance interferon signaling and control viral infection, Nat. Immunol. 16 (2015) 1215–1227.

[79] B. Luscher, I. Ahel, M. Altmeyer, A. Ashworth, P. Bai, P. Chang, M. Cohen, D. Corda, F. Dantzer, M.D. Daugherty, T.M. Dawson, V.L. Dawson, S. Deindl, A. R. Fehr, K. Feijs, D.V. Filippov, J.P. Gagne, G. Grimaldi, S. Guettler, N.C. Hoch, M.O. Hottiger, P. Korn, W.L. Kraus, A. Ladurner, L. Lehtio, A. Leung, C.J. Lord, A. Mangerich, I. Matic, J. Matthews, G.L. Moldovan, J. Moss, G. Natoli, M.L. Nielsen, M. Niepel, F. Nolte, J. Pascal, B.M. Paschal, K. Pawlowski, G.G. Poirier, S. Smith, G. Timinszky, Z.Q. Wang, J. Yelamos, X. Yu, R. Zaja, M. Ziegler, ADP-ribosyltransferases, an update on function and nomenclature, FEBS J. 289 (2022) 7399–7410.

[80] S. Vyas, I. Matic, L. Uchima, J. Rood, R. Zaja, R.T. Hay, I. Ahel, P. Chang, Family-wide analysis of poly(ADP-ribose) polymerase activity, Nat. Commun. 5 (2014) 4426.

[81] N. Dukic, O. Stromland, J.D. Elsborg, D. Munnur, K. Zhu, M. Schuller, C. Chatrin, P. Kar, L. Duma, O. Suyari, J. Rack, D. Baretic, D. Crudgington, J. Groslambert, G. Fowler, S. Wijngaarden, E. Prokhorova, J. Rehwinkel, H. Schuler, D.V. Filippov, S. Sanyal, D. Ahel, M.L. Nielsen, R. Smith, I. Ahel, PARP14 is a PARP with both ADP-ribosyl transferase and hydrolase activities, Sci. Adv. 9 (2023) eadi2687.

[82] D.A. Hume, S.M. Millard, A.R. Pettit, Macrophage heterogeneity in the single-cell era: facts and artifacts, Blood 142 (2023) 1339–1347.